

## Aura Microwave Limb Sounder observations of the polar middle atmosphere: Dynamics and transport of CO and H<sub>2</sub>O

Jae N. Lee,<sup>1</sup> Dong L. Wu,<sup>1</sup> Gloria L. Manney,<sup>1,2</sup> Michael J. Schwartz,<sup>1</sup> Alyn Lambert,<sup>1</sup> Nathaniel J. Livesey,<sup>1</sup> Kenneth R. Minschwaner,<sup>2</sup> Hugh C. Pumphrey,<sup>3</sup> and William G. Read<sup>1</sup>

Received 22 June 2010; revised 22 October 2010; accepted 29 December 2010; published 8 March 2011.

[1] The vertical structure and evolution of the wintertime annular modes are studied using 6 years of geopotential height, carbon monoxide (CO), and water vapor (H<sub>2</sub>O) data from Aura Microwave Limb Sounder. The Northern Hemisphere annular mode (NAM) and the Southern Hemisphere annular mode (SAM) reveal a strong coupling of the dynamics in the stratosphere and mesosphere between 316 hPa (~9 km) and 0.002 hPa (~90 km). CO is a good tracer throughout the middle atmosphere, while variable vertical gradients of H<sub>2</sub>O limit the regions where it is useful as a dynamical tracer. The maximum of the CO NAM and SAM (CNAM and CSAM) indices is used to monitor and characterize the evolution of wintertime polar dynamics as a function of time and height. The CNAM analysis reveals reformation of a stronger mesospheric polar vortex after significant stratospheric sudden warmings in 2006, 2009, and 2010. There is a significant anticorrelation between the mesospheric and stratospheric CNAM indices during 2005–2010 winters, supporting the hypothesis of mesosphere–stratosphere coupling through planetary-gravity wave interactions.

**Citation:** Lee, J. N., D. L. Wu, G. L. Manney, M. J. Schwartz, A. Lambert, N. J. Livesey, K. R. Minschwaner, H. C. Pumphrey, and W. G. Read (2011), Aura Microwave Limb Sounder observations of the polar middle atmosphere: Dynamics and transport of CO and H<sub>2</sub>O, *J. Geophys. Res.*, 116, D05110, doi:10.1029/2010JD014608.

### 1. Introduction

[2] The middle atmosphere is an important region where wave propagation, dynamical coupling, and tracer transport affect both the lower and upper atmospheres; it acts as transition zone between the photochemically driven ionosphere [Goncharenko *et al.*, 2010] and the wave generating troposphere. Dynamics in the middle atmosphere determine the extent and timing of polar processes, ozone chemistry, and composition distribution [e.g., Lahoz *et al.*, 2009].

[3] Forced by upper tropospheric weather systems or internal instabilities, extratropical planetary and gravity waves can propagate upward and reach the mesosphere with growing amplitudes, becoming the dominant dynamical forcing in the upper atmosphere [Wu, 2000; Salby *et al.*, 2002; Pancheva *et al.*, 2008; Harvey *et al.*, 2009; Offermann *et al.*, 2009]. Wave-induced forcings in the polar region can drive a meridional circulation that causes upwelling in the tropical stratosphere, poleward and down-

ward in the extratropics [Garcia and Boville, 1994; Holton *et al.*, 1995]. Thus, the wave forcings act as a downward control to the equatorial troposphere and can further enhance or reduce the small-scale waves and cirrus clouds there [Eguchi and Kodera, 2007].

[4] The middle atmosphere wintertime dynamics are dominated by the polar vortex, a strong band of circumpolar westerly winds that forms from the balance between the Coriolis force and radiative forcing [e.g., Schoeberl *et al.*, 1992]. Observations of and model results for the polar vortex and its variability are often analyzed with either a vortex-centered perspective using, e.g., vortex averages and equivalent latitude [e.g., Manney *et al.*, 2005, 2009a, 2009b] or along-orbit perspective views [Lahoz *et al.*, 2009, and references therein], or from a zonal mean and planetary-scale (wave numbers 1 to 3) wave decomposition [e.g., Manney *et al.*, 2008a, 2009a; Siskind *et al.*, 2007, 2010, and references therein].

[5] Another way of looking at dynamical perturbations in the winter polar regions is to project the variability in geopotential height (GPH) onto empirical orthogonal functions (EOFs) [e.g., Thompson and Wallace, 1998, 2000; Limpasuvan and Hartmann, 1999; Baldwin and Dunkerton, 1999, 2001; Ruzmaikin and Feynman, 2002; Thompson *et al.*, 2005; Gerber *et al.*, 2010]. The first EOF mode, referred to the Northern or Southern Hemisphere annular mode (NAM and SAM), is an approximately axially symmetric structure between high latitude and

<sup>1</sup>Jet Propulsion Laboratory, California Institute of Technology, Pasadena, California, USA.

<sup>2</sup>Department of Physics, New Mexico Institute of Mining and Technology, Socorro, New Mexico, USA.

<sup>3</sup>Institute of Atmospheric and Environmental Sciences, School of GeoSciences, University of Edinburgh, Edinburgh, UK.

midlatitude and has been used to monitor the strength of the winter polar vortex. *Lee et al.* [2009] show the first six EOF modes of the Aura Microwave Limb Sounder (MLS) GPH observations up to mesopause during extreme events such as stratospheric sudden warmings (SSWs).

[6] Above the stratosphere, observations of the polar vortex have been limited, but vertical descent from the mesospheric into the stratospheric vortex has been studied with various models and data [e.g., *Fisher et al.*, 1993; *Manney et al.*, 1994, 1995; *Rosenfield et al.*, 1994; *Bacmeister et al.*, 1995; *Eluszkiewicz et al.*, 1995; *Abrams et al.*, 1996a, 1996b; *Allen et al.*, 2000; *Kawamoto and Shiotani*, 2000]. *Fisher et al.* [1993] analyzed three-dimensional winds from a mechanistic model of the stratosphere and mesosphere to describe the general features of large-scale air motion through the course of an idealized austral winter. *Manney et al.* [1994] and *Rosenfield et al.* [1994] estimated the diabatic descent rates at several altitudes within the polar vortices by calculating diabatic cooling for ensembles of trajectories in the vortex using winds and temperatures from the Met Office stratosphere-troposphere data assimilation system analyses. *Manney et al.* [1995] estimated the vertical descent inside the polar vortex from Lagrangian transport calculations using Upper Atmosphere Research Satellite (UARS) Microwave Limb Sounder (MLS) and Cryogenic Limb Array Etalon Spectrometer (CLAES) tracer observations.

[7] Unusual vertical displacement of the winter Arctic stratopause and anomalous descent of mesospheric air following the strong, prolonged SSW in 2006 are shown and compared to 2005 by *Siskind et al.* [2007]. Using the data from Sounding of the Atmosphere with Broadband Emission Radiometry (SABER) experiment on the NASA/Thermosphere Ionosphere Mesosphere Energetics and Dynamics (TIMED) satellite and simulations from the NOGAPS-ALPHA (Navy Operational Global Atmospheric Prediction System–Advanced Level Physics High Altitude), they found that polar descent in strong reformed vortex after the SSW in 2006 was much stronger than that at a similar time in the cold, relatively undisturbed 2005 winter, and suggested that gravity waves modulated by planetary waves were important in coupling the stratosphere and the upper atmosphere.

[8] Aura MLS data can provide new insights on the polar vortex dynamics throughout the middle atmosphere by extending the GPH, temperature, and trace gas measurements from the upper troposphere to the mesopause. MLS CO volume mixing ratio (VMR) shows a large vertical gradient, with values from ppmv (parts per million by volume) in the mesosphere to ppbv (parts per billion by volume) in the low stratosphere (Figures 1a and 1c). While some CO is produced by the oxidation of methane in the stratosphere, most of stratospheric and mesospheric CO is created by photolysis of carbon dioxide in the upper mesosphere and thermosphere and transported downward into the lower mesosphere and stratosphere [*Solomon et al.*, 1985; *Allen et al.*, 1999].

[9] The main loss mechanism is oxidation by the OH radical. In the polar night, mesospheric CO is conserved due to lack of OH. Therefore, the diurnal cycle in CO VMR is small and its concentration can be used as a good tracer of atmospheric dynamics in both day and night, particularly for the wintertime polar dynamics.

[10] The balance between the source and the sink leads to the strong vertical gradient of CO mixing ratios with relatively abundant CO in the upper mesosphere, but with extremely small VMRs in the lower stratosphere (Figures 1a and 1c). Horizontal CO gradients reflect the transport in the winter polar vortex. The descent in the polar region brings high CO from the mesosphere to the lower stratosphere. Since the CO lifetime is over 30 days in the polar stratosphere and mesosphere during winter [*Minschwaner et al.*, 2010], it is long enough to maintain the horizontal gradient between low CO outside the vortex and high CO inside. It has a relatively shorter lifetime (about 10 days) at the low latitudes and midlatitudes in the middle to upper stratosphere, which helps to remove CO quickly once it is mixed out of the vortex.

[11] It will be shown in section 4 that meridional CO gradients decrease in the stratosphere (below ~1 hPa) during strong SSWs, but stronger gradients begin to build up in the mesosphere 4–5 days after the SSW. The high CO VMR transported down to the stratospheric polar vortex does not disappear immediately after the SSW events. Breaking planetary waves may help to mix it with the midlatitude air, causing a slight increase of midlatitude CO. However, the short (~10 days) lifetime there makes CO gradually disappear.

[12] The H<sub>2</sub>O VMR decreases (Figures 1b and 1d) with height in the mesosphere where it is influenced by solar Lyman  $\alpha$  flux as a sink through the photolysis. However, the solar influence on the water vapor VMR becomes less significant below ~80 km [*Grygalashvily and Sonnemann*, 2006]. In the middle and lower stratosphere, water vapor abundance is affected by many factors, including the descent from the mesosphere, transport from the tropical tropopause through the Brewer Dobson circulation [*Randel et al.*, 1993, 2006], chemical formation from oxidation of methane, and dehydration via sedimenting of polar stratospheric clouds (PSCs) during winter.

[13] The chemical lifetime of water vapor in the middle atmosphere is of the order of years in the lower stratosphere (in absence of PSC processing) and months in the lower mesosphere [*Brasseur and Solomon*, 2005]. Because of different vertical gradients of H<sub>2</sub>O VMR above and below its peak in the upper stratosphere, H<sub>2</sub>O concentrations carry different dynamical signatures depending on the altitude range. The dry air from the mesosphere can be used as a dynamical tracer to examine the polar descent from the upper atmosphere. Conversely, in the lower and middle stratosphere, the descent of moist air can be used as a tracer of transport. In the upper stratosphere where H<sub>2</sub>O abundance peaks, H<sub>2</sub>O is not a good tracer.

[14] The zonal mean H<sub>2</sub>O distribution in the stratosphere is nearly symmetric about the equator during the boreal winter (Figure 1b), but is slightly asymmetric during the austral winter (Figure 1d). During the austral winter, moist air extends below 10 hPa in the Southern Hemisphere polar region while it is confined above 5 hPa in the boreal winter.

[15] To better understand dynamical variability of the wintertime polar middle atmosphere, we analyze Aura MLS GPH, CO and H<sub>2</sub>O measurements to examine middle atmosphere dynamics and transport from the mesopause to the upper troposphere. We extract the EOF modes for GPH, CO, and H<sub>2</sub>O at each MLS retrieval pressure to study mesosphere–stratosphere coupling and descent in the polar

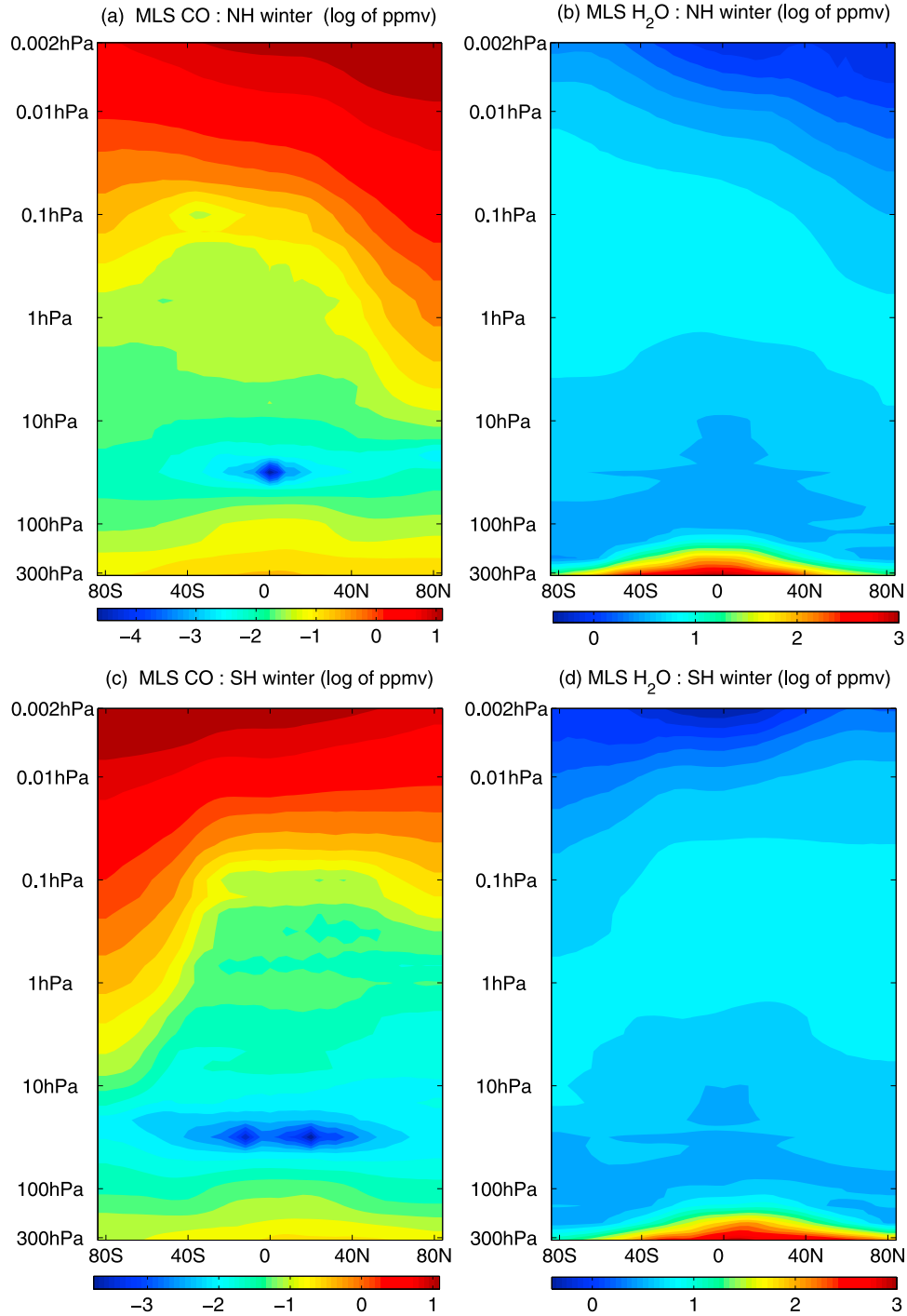


**Figure 1.** Zonal mean MLS CO and H<sub>2</sub>O VMR in log ppmv (parts per million by volume) as a function of latitude (a, b) for the NH and (c, d) for the SH winters. DJF for 2005–2010 and JJA for 2005–2009 are averaged for the NH and SH, respectively.

vortex in the 2005–2010 winters (2005–2009 winters for the Southern Hemisphere).

## 2. Data and Methods

### 2.1. Data

[16] The MLS data used in this study are the version 2.2 (v2.2) daily GPH, CO and H<sub>2</sub>O, gridded separately for day

and night, which have 35 pressure levels from the upper troposphere (316 hPa) to the mesopause ( $\sim 0.001$  hPa/ $\sim 0.002$  hPa for H<sub>2</sub>O and CO). Although we have also examined other MLS trace gas measurements, in this study we present the results for GPH, CO, and H<sub>2</sub>O. The daily GPH, CO, and H<sub>2</sub>O fields are mapped onto a  $4^\circ$  (latitude)  $\times$   $8^\circ$  (longitude) grid for daytime (ascending) and nighttime (descending) orbits. Because Aura MLS sampling does not

cover the regions poleward of 82° latitude, the observations in latitude bins between 20°N and 82°N for NH (20°S and 82°S for SH) during the winter months (November to March for NH; May to October for SH) are used to derive the winter EOF modes.

[17] MLS GPH accuracy and precision are ~100 m in the middle stratosphere and ~150 m at 316 hPa. The MLS GPH low bias with respect to SABER, which increases with height, is estimated to be 100 m or less for 10–0.046 hPa, and 500–750 m at 0.001 hPa; an overall bias, however, has little impact on the anomaly fields used to calculate the EOFs. Details on validation of the MLS geopotential height field and temperature are discussed by *Schwartz et al.* [2008]. Typical precision values of the MLS V2.2 CO vary from 0.02 ppmv at 100 hPa, 0.2 ppmv at 1 hPa, to 11 ppmv at 0.002 hPa, with vertical resolution of 4, 3, and 9 km, respectively [*Pumphrey et al.*, 2007]. Typical precision values of the MLS V2.2 water vapor are 0.3–2 ppmv over the range of 68 to 0.002 hPa with vertical resolution of 3–4 km at pressures >2 hPa, 5–7 km at 1–0.2 hPa, and 12–16 km at pressures <0.1 hPa [*Lambert et al.*, 2007].

## 2.2. Method

[18] To characterize wintertime polar variability, we apply an EOF analysis as described by *Baldwin and Dunkerton* [1999, 2001] and compute the EOF modes from daily gridded MLS GPH and tracers observations. The EOF analysis is carried out independently for each altitude from the daily measurements of the entire winter period (November to March). A wintertime mean of the MLS data is removed for each grid cell before calculating the EOF modes of GPH, H<sub>2</sub>O, and CO anomalies. Details of the EOF calculation from the MLS GPH and its comparison with that obtained from the longer-term analysis are discussed by *Lee et al.* [2009].

## 3. Empirical Orthogonal Function Analysis of GPH, CO, and H<sub>2</sub>O

### 3.1. EOF Patterns

[19] Figures 2 and 3 show the first three EOF patterns of GPH and CO at 0.1 hPa for the NH winter and SH winter, respectively. Two additional stratospheric levels, 10 hPa and 56 hPa (4.6 hPa and 56 hPa in the SH), are used to show H<sub>2</sub>O variations because of its changing horizontal and vertical gradients. The first EOF mode of GPH, called the Northern Annular Mode (NAM) in the NH and the Southern Annular Mode (SAM) in the SH, represent an approximately axially symmetric annular structure of the polar vortex (Figures 2a and 3a), reflecting minimum of the mean GPH field at winter pole.

[20] Similarly, the first EOF modes of CO and H<sub>2</sub>O are defined as CNAM and HNAM in the NH and CSAM and HSAM in the SH (Figures 2b–2e and 3b–3e). The first EOF of CO (CNAM and CSAM) in the middle atmosphere is an approximately axially symmetric annular pattern with a “dome-like” shape centered on the pole, reflecting high CO VMR in high latitudes decreasing with decreasing latitude.

[21] The middle atmospheric circulation results in low H<sub>2</sub>O VMR in the winter polar mesosphere due to descent from the mesopause and high H<sub>2</sub>O VMR in the summer polar mesosphere [*Andrews et al.*, 1987] due to ascent from

the stratosphere. Thus the first EOF of H<sub>2</sub>O (HNAM and HSAM) in the mesosphere is also an annular pattern with “well-like” shape centered on the pole, reflecting a mean distribution of H<sub>2</sub>O that is dry at high latitudes and moist at low latitudes (Figures 2c and 3c).

[22] The second and third modes of the NAM, SAM, CNAM, and CSAM can be viewed as a pair of wave 1 patterns with the orthogonal orientation rotating slightly with altitude. Similar ranking of EOF patterns has been noted in NH column ozone [*Jiang et al.*, 2008]. For the HNAM and HSAM (Figures 2c–2e and 3c–3e), the second EOFs have an annular pattern at high latitudes transitioning to a wave 1 pattern at midlatitudes. The EOF modes in the trace gases reflect the strengthening and weakening of anomalies as in the GPH modes since strong vortices are associated with stronger tracer gradients along their edge. However, unlike the GPH EOF modes, which are forced from the lower atmosphere, the CO EOF modes also carry a fingerprint of perturbations from the thermosphere and upper mesosphere as a result of descent. Similarly, the mesospheric H<sub>2</sub>O EOF modes reflect changes in the anomaly strength/sign and the descent of perturbation patterns originating in the upper mesosphere; the lower stratospheric H<sub>2</sub>O patterns are associated with upward propagating planetary waves (Figures 5c and 9c).

[23] The first EOF of GPH in the SH (SAM) accounts for up to 90% (60% in the NH (NAM)) of the total variance in the middle atmosphere before decreasing in the upper mesosphere (above ~0.01 hPa). Considering the fact that the mode is calculated from every grid point between 20°S and 82°S, capturing 90% of variance in a single in a single EOF mode is exceptional. It captures less variability near 300 hPa than does the NAM (which explains ~17% of the variability at this level), explaining less than 15%, of the variability. Details of the vertical distribution of variance of the NAM are explained by *Lee et al.* [2009]. As expected given the stronger and more symmetric SH polar vortices, the SAM captures more variance than the NAM in the upper stratosphere and mesosphere. However, it explains less variance than the NAM at levels below ~10 hPa.

[24] The CNAM and CSAM explain more than 60% of the variance at ~10 hPa in both hemispheres, but the percentage decreases steadily with increasing height to ~0.01 hPa. Below 50 hPa, these modes represent less than 17% of the total variance, likely due to the diminishing MLS sensitivity to CO and very low CO mixing ratios.

[25] The amount of variance accounted for by the HNAM varies strongly with height and has peaks near 0.1 hPa and 1 hPa that explain ~60% of the total variance at those levels. The HSAM accounts for the most variance, ~50%, near 0.01 hPa (Figure 4m). The spatial patterns and variances of the HNAM and HSAM are quite different reflecting different distribution of H<sub>2</sub>O between the NH and SH. Variances explained by the HSAM are larger in the middle and lower stratosphere than those of HNAM, consistent with larger planetary wave amplitudes in the NH stratosphere. The variance explained by the first mode of H<sub>2</sub>O is less than that from GPH, possibly due in part to local variability caused by the interplay between chemistry and dynamics [e.g., *Flury et al.*, 2008; *Remsberg*, 2010].

[26] The first EOF modes from the GPH, CO, and H<sub>2</sub>O are significant at all MLS pressure levels. According to the

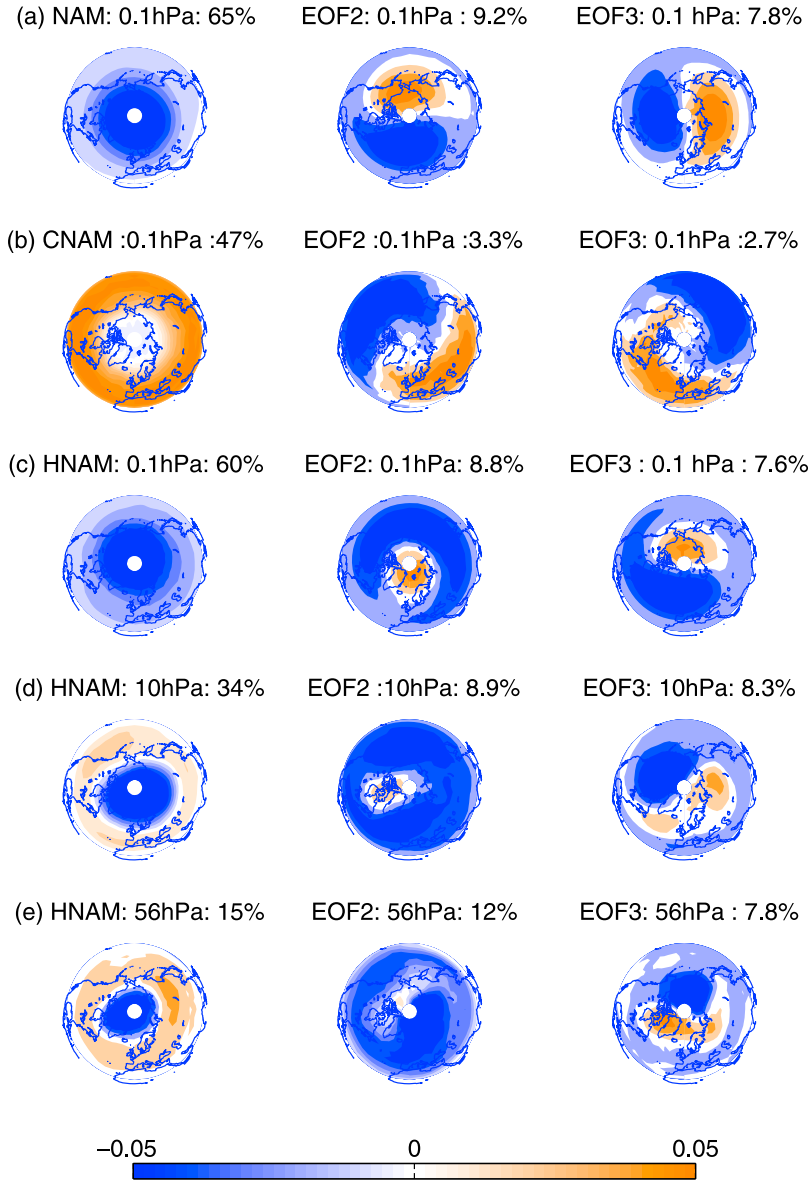


**Figure 2.** First three winter EOF modes from MLS GPH, CO, and H<sub>2</sub>O during boreal winters (NDJFM) at 0.1 hPa (two more stratospheric levels for H<sub>2</sub>O). The first EOF modes of GPH, CO, and H<sub>2</sub>O are defined as the NAM, CNAM, and HNAM in the NH. Numbers in percent indicate variance represented by each mode to the total variance.

criterion of *North et al.* [1982], the eigenvalues ( $\lambda_k$ ) of the EOF modes have sampling uncertainties  $\Delta\lambda_k \sim \lambda_k \sqrt{2/N}$  when the covariance matrix is constructed on the basis of  $N$  independent samples. A similar amount of variance is explained by the second and third modes, suggesting that these modes are closely connected to each other.

### 3.2. Indices of the Modes

[27] The index of the principal component in GPH, generated by regressing daily data onto the spatial pattern of the first EOF, has been quite useful (1) to monitor the strength of the daily polar vortex variations and (2) to track the vortex evolution with time and height [Lee *et al.*, 2009]. Calculating an analogous, dimensionless index from trace

gas mixing ratios can help characterize the dynamical structures or processes controlling them at different altitudes. For example, the CO mixing ratio can vary from many ppmv in the mesosphere to a few ppbv in the low stratosphere, thus requiring appropriate scaling to compare the structures between these regions using conventional analysis methods, whereas the dimensionless index can be compared directly over a broad altitude range.

[28] Cross sections of MLS GPH, CO, and H<sub>2</sub>O composites in the extreme positive and negative phases are shown in Figure 4 for both hemispheres. The extreme positive, or very strong vortex, phase is defined by a NAM index more than one standard deviation above the mean of the 6 years (5 years for the SH) of winter index values. The extreme

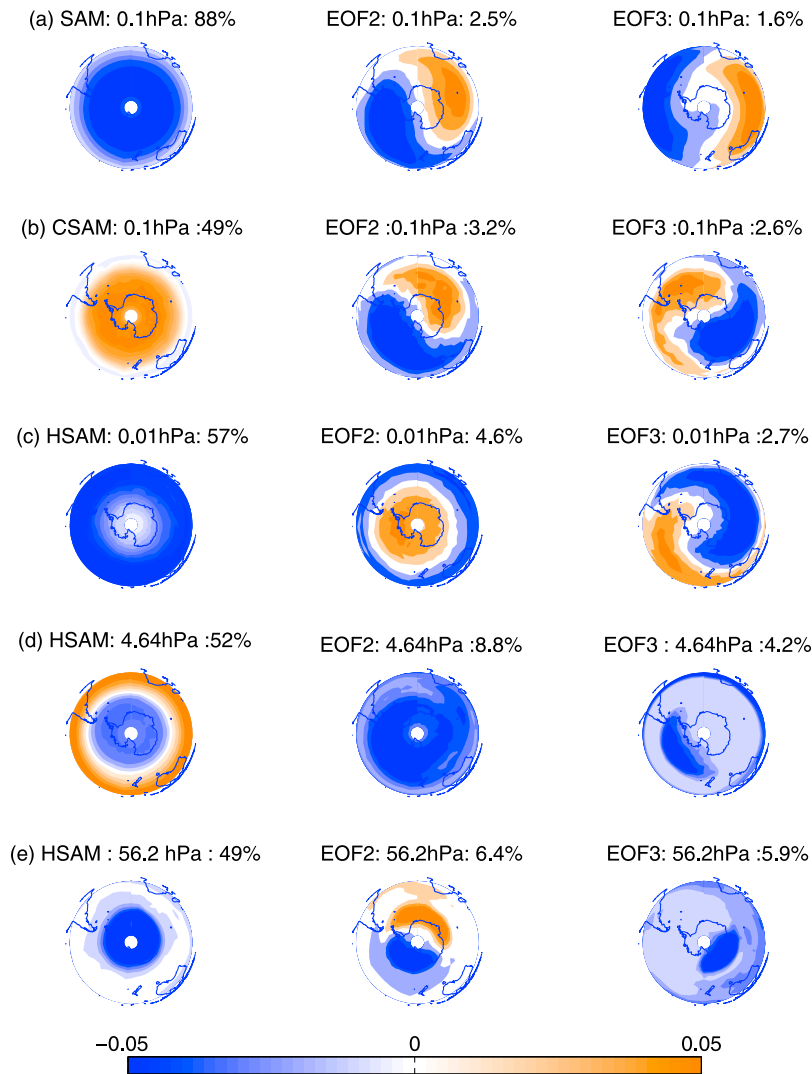


**Figure 3.** As in Figure 2 but for the SH during austral winters (MJJASO) and at 0.01 hPa, 4.6 hPa, and 56.2 hPa for  $\text{H}_2\text{O}$ . The first EOF modes of GPH, CO, and  $\text{H}_2\text{O}$  are defined as the SAM, CSAM, and HSAM in the SH.

negative, or very weak vortex, phase is similarly defined by an index more than one standard deviation below the mean. In the positive phase, GPH in the mesosphere decreases poleward with a “well-like” shape centered on the pole, a manifestation of a strong winter polar vortex in the middle atmosphere (Figure 4b). The negative NAM phase is characterized by a shallow, less defined “well,” the case of a weak vortex (Figure 4a).

[29] The positive index of CNAM represents abundant CO mixing ratios in high latitudes (Figure 4e), indicating strong descent within the strong vortex represented by the concurrent positive GPH NAM index. In the mesosphere, the mean structures of the  $\text{H}_2\text{O}$  composite are similar to those of CO, but meridional gradients of the abundance are reversed. The positive index of HNAM represents low mixing ratios of water vapor at high latitudes in the mesosphere, with a strong meridional gradient from pole to low latitudes (Figure 4h), again consistent with strong descent. The strength of the signature of confined descent in the

vortex during different NAM phases is reflected in the latitudinal CO and  $\text{H}_2\text{O}$  gradients (Figures 4b, 4e, and 4h): More pronounced gradients across the NH and SH in the strong vortex case arise from an undiluted signature of strong descent when air is well confined within a strong vortex. The positive phase of CNAM and HNAM in the mesosphere corresponds to less horizontal transport of the tracers from low to high latitudes with a well-developed polar vortex, while the negative phase corresponds to enhanced latitudinal transport and a less distinct signature of confined descent within a weaker, more permeable, polar vortex.

[30] In the stratosphere,  $\text{H}_2\text{O}$  mixing ratios increase due to its formation from oxidation of methane, and reach a maximum near the stratopause and in the lower mesosphere. Below 5 hPa, the vertical gradient of water vapor is reversed from that of the mesosphere. Thus, the negative phase of the HNAM index below 10 hPa appears as a well-defined “dome-like” structure centered on the pole, which represents

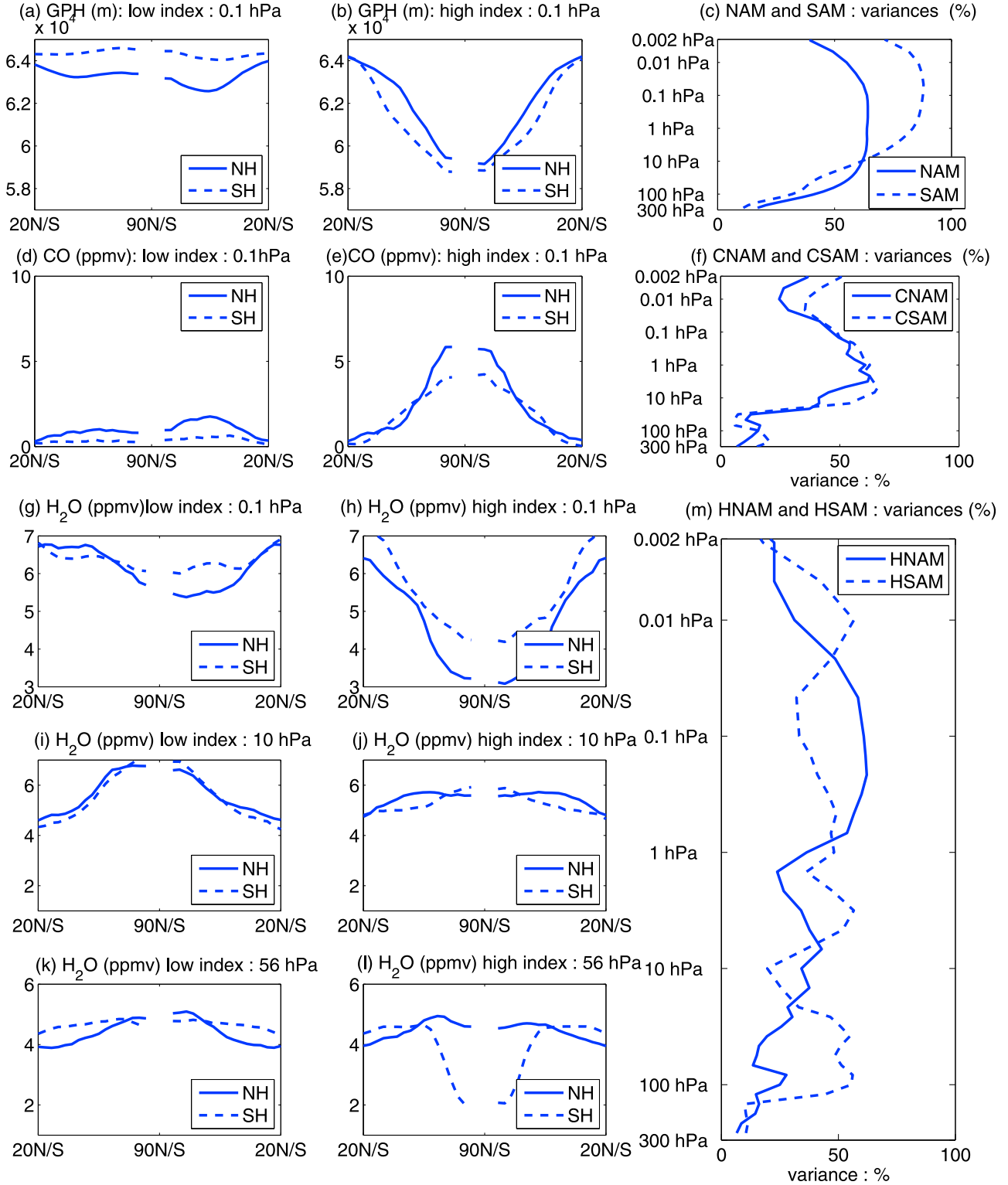


**Figure 4.** Cross sections of the MLS GPH, H<sub>2</sub>O, and CO composites across 90°W–90°E in both hemispheres for high and low indices of the first EOF mode for (a, b) GPH (in m), (d, e) CO (in ppmv) at 0.1 hPa, and (g, h, l) H<sub>2</sub>O (in ppmv) during the winter period (NDJFM for the NH and MJJASO for the SH). Variances of the each first mode of (c) NAM and SAM, (f) CNAM and CSAM, and (m) HNAM and HSAM are also shown.

**Table 1.** Regression Coefficient of Descent Rate  $\log_{10} P(t) = p_0 + p_1 t + p_2 t^2 + p_3 t^3 + p_4 t^4$ , Estimated From a Fourth-Order Polynomial Function of the Averaged CO Index Maxima, as a Function of Time (day)

	Regression Coefficients for $P(t)$
NH mesospheric late descent <sup>a</sup>	$p_0 = -43.671$ $p_1 = 1.487$ $p_2 = -0.019$ $p_3 = 1.039\text{e-}04$ $p_4 = -1.944\text{e-}07$
NH stratospheric early descent <sup>b</sup>	$p_0 = -0.307$ $p_1 = 0.042$ $p_2 = -9.487\text{e-}04$ $p_3 = 1.243\text{e-}05$ $p_4 = -5.615\text{e-}08$
SH <sup>c</sup>	$p_0 = -2.623$ $p_1 = 0.073$ $p_2 = -6.679\text{e-}04$ $p_3 = 3.069\text{e-}06$ $p_4 = -5.274\text{e-}09$

<sup>a</sup>Day 65 to day 112; day 1 begins at first of December.  $P(t)$  is averaged for strong SSW years (2006 and 2009).

<sup>b</sup>Day 1 to day 110; day 1 begins at first of December.  $P(t)$  is averaged for 2005, 2007, 2008, and 2010.

<sup>c</sup>Day 1 to day 180; Day 1 begins at first of May.  $P(t)$  is averaged for 2005–2009.

high mixing ratio in high latitudes with stronger latitudinal gradient (Figures 4i–4j). The high index still represents low mixing ratios, but with weaker latitudinal gradients (a lower “dome”). In the positive phase of HSAM at 56 hPa level, strong meridional gradients from pole to high latitudes are observed (Figure 4l) because of the loss of water vapor in the cold SH lower stratospheric polar vortex via PSC processes (sequestration and/or dehydration), whereas weak gradients are observed in the HNAM case since there is much less extensive PSC activity in the warmer NH lower stratospheric vortex. Stronger horizontal transport from low latitudes due to planetary wave activity in the NH [e.g., Randel *et al.*, 1993] is reflected in the composited  $\text{H}_2\text{O}$  distribution and in the low percentage (~15%) of the total variance explained by the HNAM (Figure 4m).

### 3.3. Estimate of Descent of Anomaly Index

[31] The maximum CNAM/CSAM index can be used to monitor evolution of the middle atmospheric dynamics since the primary CO source is thermospheric photolysis of  $\text{CO}_2$  [Solomon *et al.*, 1985]. With a long lifetime in the middle atmosphere during winter, CO is a good tracer of transport in the polar vortex. If the polar descent in the winter occurs without significant horizontal mixing or chemical or photochemical losses, that diabatic descent will fill the vortex to progressively lower altitudes with high CO from above, as is represented in the first EOF mode. Thus, CO descending through the mesosphere into the stratospheric vortex will be reflected in descent of CO index contours. Because the maximum index may also descend if the anomaly strengthens at progressively lower levels (as would, for example, be expected when the vortex forms starting first at the top), the descent rate of the index typically will not represent solely the material descent rate; the extent to which it does so provides information on the relative importance of the two processes to the evolution of the index.

[32] Thus, although the CNAM/CSAM is a good indicator of winter polar dynamics, its evolution cannot necessarily be interpreted as a quantitative measure of the material descent since chemical processes and dynamical processes not directly related to descent may also affect the CNAM/CSAM changes. On the other hand, unlike methods using individual profiles inside the vortex [e.g., Kawamoto and Shiotani, 2000], our approach derives the descent rate based on the entire high-latitude structure, representing an average rate of the polar CO changes. Some studies have used “vortex-averaged descent” methods using trace gas data to estimate the descent inside the vortex [e.g., Schoeberl *et al.*, 1992; Tuck *et al.*, 1993; Russell *et al.*, 1993]. Those studies, however, were typically confined to the middle and/or lower stratosphere, and often hampered by sparse data.

[33] To estimate descent of the CNAM index, the pressure level of the CO index maximum in each winter as a function of time (day) is regressed onto a fourth-order polynomial function for a smooth curve  $P(t)$  from 1 December for the NH and from 1 May for the SH. The regression coefficients for  $\log_{10} P(t) = p_0 + p_1 t + p_2 t^2 + p_3 t^3 + p_4 t^4$  are listed in Table 1. The pressure level,  $P$ , is converted to a geometric height,  $Z$ , using an average DJFM temperature profile poleward of  $60^\circ\text{N}$  for the NH (MJJASO temperature poleward of  $60^\circ\text{S}$  for the SH) during 2005–2008 from the GMAO Modern Era Retrospective-Analysis For Research and Applications (MERRA) analysis up to 0.01 hPa.  $Z$  is estimated to be a function of  $\log_{10} P$ ,  $Z = -15.77 \log_{10} P + 46.03$  in the NH, and  $Z = -15.92 \log_{10} P + 45.36$  in the SH, when  $P$  is from 0.02 hPa to 165 hPa.

[34] The curve of  $Z(t)$  is then converted to a descent rate at a particular height at each time since each  $Z(t)$  curve passes a particular altitude on a particular day of the year. Thus we derive the descent rate  $w(t) = dZ(t)/dt = [Z(\text{day} + 1) - Z(\text{day})]/\text{day}$ , which represents the descent rate at a particular altitude on a given day. This approach derives the descent rate based on the entire CNAM or CSAM structure, representing an overall or average rate of polar descent of the MLS high-latitude ( $60^\circ\text{N}$ – $82^\circ\text{N}$ ) tracers.

[35] In the SH, the descent is usually relatively continuous from the mesosphere to the upper troposphere during the winter. However, in some NH winters (2006, 2009 and 2010) there are two periods of descent, with the interruption caused by an extreme SSW. Therefore, we estimate the descent rate for two different periods in the NH: one for the stratosphere during early winter starting in December and one for the mesosphere during late winter starting in February (Table 1).

## 4. Dynamics and Transport of CO and $\text{H}_2\text{O}$

### 4.1. Northern Hemisphere

#### 4.1.1. Mesosphere

[36] Northern winter mesospheric dynamics are highly variable and are coupled to perturbations in the lower atmosphere [e.g., Andrews *et al.*, 1987; Siskind *et al.*, 2007, 2010; Coy *et al.*, 2009]. The Aura MLS observation period covers six NH winter seasons (2005–2010) during which three unusually strong and prolonged major SSWs occurred (2006, 2009 and 2010). The strong SSWs in 2006 and 2009 are associated with the cooling in the mesosphere [e.g., Manney *et al.*, 2008a, 2009b; Lee *et al.*, 2009]. Major SSWs

in January 2006 and 2009 distorted the polar vortex in a top-down progression with the vortex breakdown starting in the mesosphere, then shifting the stratospheric vortex off the pole in 2006 and splitting it in 2009. Prior to the major SSWs in 2006, 2009, and 2010, the stratospheric vortex is stronger in the upper stratosphere and lower mesosphere compared to other years as indicated by the CNAM index, with associated stronger descent in this region (Figure 5b), as in the work of *Manney et al.* [2008b] and *Siskind et al.* [2007, 2010].

[37] The NAM from MLS GPH captures the dominant patterns of interannual variability in middle atmospheric dynamics. Positive phases of the NAM index are predominant in the mesosphere after January during 2005, 2007, and 2008 (the relatively quiescent winters), whereas strong and persistent negative phases of the NAM were seen in the stratosphere throughout January 2006, 2009, and 2010 (Figure 5a) during the strong SSW events. The negative NAM winters are characterized by a weakened mesospheric polar vortex with significant easterly anomalies extending down to the upper stratosphere in January 2006, 2009, and 2010. However, the positive NAM development in the mesosphere is weaker during the SSW in 2010 than during the SSWs in 2006 and 2009. Detailed characterization of the SSW in 2010 and comparison with previous warmings is a subject of ongoing investigations.

[38] Comparison of the time height evolution of CNAM and HNAM indices shows distinct and concurrent positive phases (Figures 5b and 5c) developing near the mesopause in February of 2006 and 2009 after the SSWs. The descent of a reforming vortex in the lower mesosphere and the upper stratosphere in the 2010 winter shows a similar pattern to the previous SSWs of 2006 and 2009, but with a substantially weaker signal than those (Figure 5a).

[39] The timing of the NAM index switching from positive to negative varies from year to year. In 2006 and 2009, strong and persistent positive water vapor and CO regimes above 0.1 hPa are coincident with development of the positive mode of geopotential height during February 2006 and 2009. In early February of 2006 and 2009 the positive index of the HNAM (Figure 5c) shows rapid descent of low water vapor from the upper mesosphere. It reflects a reforming vortex in the lower mesosphere and eventually in the upper stratosphere, with mesospheric air (low H<sub>2</sub>O, high CO) filling the vortex after the SSWs [e.g., *Manney et al.*, 2009a, 2009b]. As the positive NAM signals progress downward until mid-February in 2006 and late February in 2009 to ~1 hPa level, the strong positive signals in CO and H<sub>2</sub>O also progress until end of March of 2006 and 2009. Similar positive signals in CO and H<sub>2</sub>O are shown in 2010 even though the positive NAM development in the mesosphere is weaker during the SSW in 2010 than during the SSWs in 2006 and 2009.

#### 4.1.2. Stratosphere

[40] The downward progression of the CNAM maxima in Figure 5b shows two periods of strong descent of the index associated with the two distinct confined descent periods in fall/early winter as the vortex strengthens, and during the reformation of the vortex after the SSW. The positive values in early February 2006, 2009, and 2010 descend from the lower mesosphere to the stratosphere (~10 hPa) following the SSWs while a vortex is forming in the mesosphere and upper stratosphere. The progression of the positive index values below 1 hPa reflects descent of high CO concentration from the upper stratosphere and lower mesosphere (USLM) to the stratosphere (~10 hPa) as stratospheric vortex is forming in early winter; the strengthening of the vortex at progressively lower levels may also contribute to the descent of the CO index maxima.

[41] During the strong SSW years (2006 and 2009), as revealed by the CNAM index maximum, the early vortex descent is interrupted before reaching the midstratosphere (~10 hPa). The descent in nonwarming years, on the other hand, can continue down to the ~10 hPa level by early March. The USLM descent is interrupted before February while a positive CNAM index (i.e., strong vortex) is being developed in the mesosphere. In 2010 winter, unlike other winters with strong prolonged SSWs, the USLM descent continues into March, since the mesospheric vortex development is not strong enough to interrupt the early descent.

[42] The CNAM analysis reveals a significant anticorrelation ( $r = -0.9$ ) between the mesospheric and stratospheric CNAM indices from 2005 to 2010 winters as shown in Figure 6. These indices are from 1 to 10 March each year, averaged at pressures between 0.1 and 0.2 hPa for the mesosphere and between 20 and 30 hPa for the stratosphere. Strong mesospheric vortices (positive indices) concurrent with weak stratospheric vortices (negative indices) in late winter are thought to result from planetary-gravity wave interactions, in which planetary waves associated with SSWs prevent gravity waves from reaching the mesosphere and allow the vortex to reform strongly in the upper mesosphere [e.g., *Siskind et al.*, 2007, 2010]. In other words, the highly disturbed lowermost stratosphere during the SSW blocks the propagation of gravity waves that normally break in the upper mesosphere region. Thus, the dynamic heating above the stratosphere is reduced, leading to a more radiatively controlled atmosphere in the mesosphere with a stronger vortex. On the other hand, when the stratosphere is less disturbed with strong vortex, gravity waves propagate to the upper mesosphere before breaking and weakening the vortex in that region.

[43] In the stratosphere, the HNAM index accounts for less variability than the CNAM index, likely because the mixing ratio increases due to the formation source from oxidation of methane: If smaller-scale variances are produced by chemical

**Figure 5.** Time-height development of the first EOF mode during boreal winters of 2005–2010, obtained from the EOF analysis of the MLS (a) geopotential height, (b) CO, and (c) H<sub>2</sub>O. Red represents positive index, which corresponds to a cold condition with the strong polar vortex for geopotential height, the dry conditions for high-latitude H<sub>2</sub>O, and abundant condition of high-latitude CO. The PCs are normalized with the standard deviation of each mode at each level to show the relative comparison of the geopotential height, CO, and H<sub>2</sub>O. Four years mean stratospheric descent (2005, 2007, 2008, and 2010) and two years mean mesospheric descent (during SSW years, 2006 and 2009) of CO index,  $P(t)$ , as a regression of CO index maximum in NH winter are indicated by black lines.

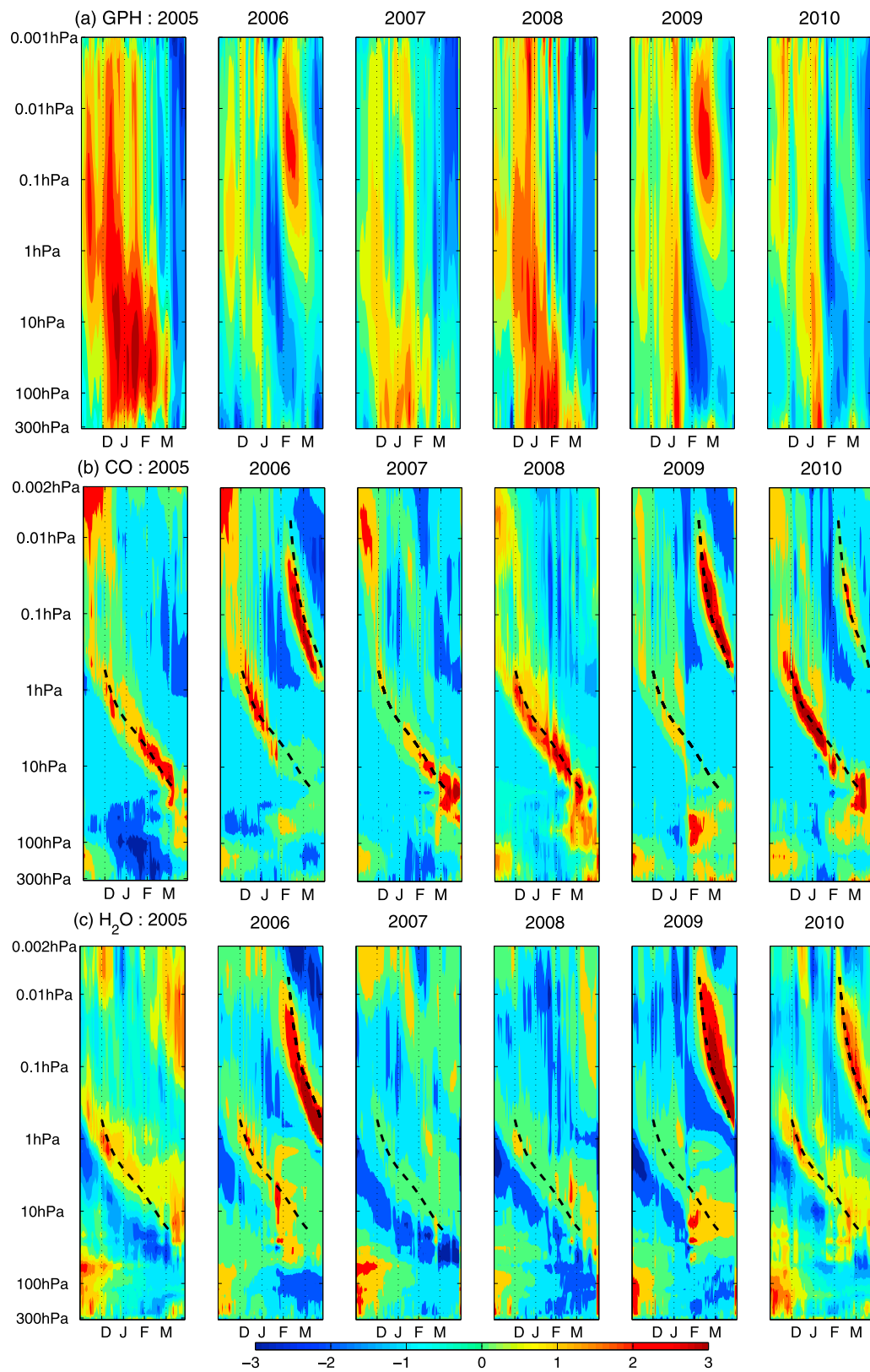
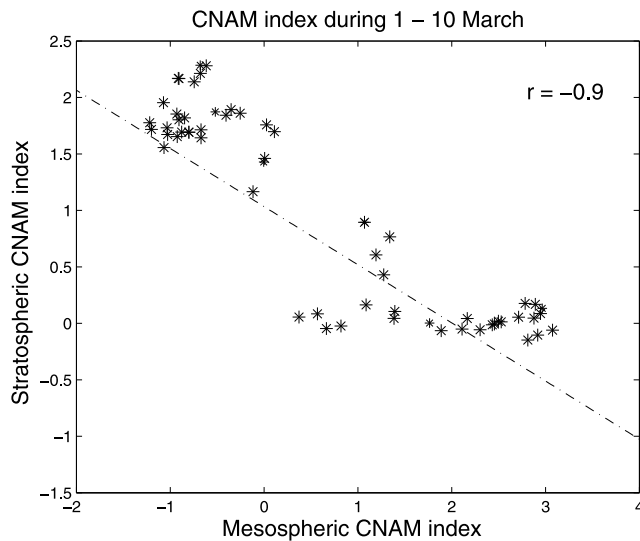


Figure 5



**Figure 6.** Relationship between the mesospheric CNAM indices and stratospheric CNAM indices during 1–10 March during 2005–2010 winters.

processes, this would reduce the fraction of variability at large scales explained by the first HNAM mode. The amount of variance explained by this mode drops to 20%–30% below 1hPa level.

#### 4.1.3. Descent and Transport of Trace Gases

[44] The descent of the CNAM index maximum,  $P(t)$ , and the rate of this descent,  $w(Z)$ , as explained in section 3, are

shown in Figure 7 for the NH winter. The pressure level of the CO index maximum in each winter, a function of time (day), is regressed to a fourth-order polynomial function for a smooth curve  $P(t)$  from 1 December (Table 1).

[45] The rates of descent of the CNAM index from the mesosphere during the SSW winters (i.e., 2006, 2009, and 2010) are similar, with the 2006 descent starting slightly earlier than that in 2009. Two years (2006 and 2009) mean HNAM index shows similar mesospheric descent to that of the CNAM index during 2006 and 2009. Generally speaking, the descent rate of the index is higher in the mesosphere and decreases linearly as altitude decreases from  $\sim 1.5$  km/d ( $\sim 45$  km/month) at 80 km to  $\sim 0.5$  km/d ( $\sim 15$  km/month) at 60 km. The typical stratospheric index descent rate during non-SSW winters is  $\sim 0.2$  km/d.

[46] The downward propagation of the maximum CNAM index shows descent of polar vortex anomaly, which can result from several processes. Wave breaking and mixing above the strongest vortex level tend to reduce tracer (CO and  $\text{H}_2\text{O}$ ) gradient and its annular mode index. Since the EOF analysis measures the contrast of tracer concentrations between  $20^\circ\text{N}$  and  $82^\circ\text{N}$ , it cannot distinguish subsidence between inside and outside of the vortex. Besides material descent in the vortex, mixing, chemistry, and subsidence outside of the vortex also can contribute to the evolution of the index.

[47] As seen in Figure 8a, the zonally averaged ( $60^\circ\text{N}$ – $82^\circ\text{N}$ ) MLS CO volume mixing ratio is between 1 and 35 ppmv in the pressure range 0.1 hPa ( $\sim 60$  km) to 0.002 hPa ( $\sim 90$  km). In the stratosphere, it is extremely low between 100 to 1000 ppbv in the pressure range 100 hPa (20 km) to

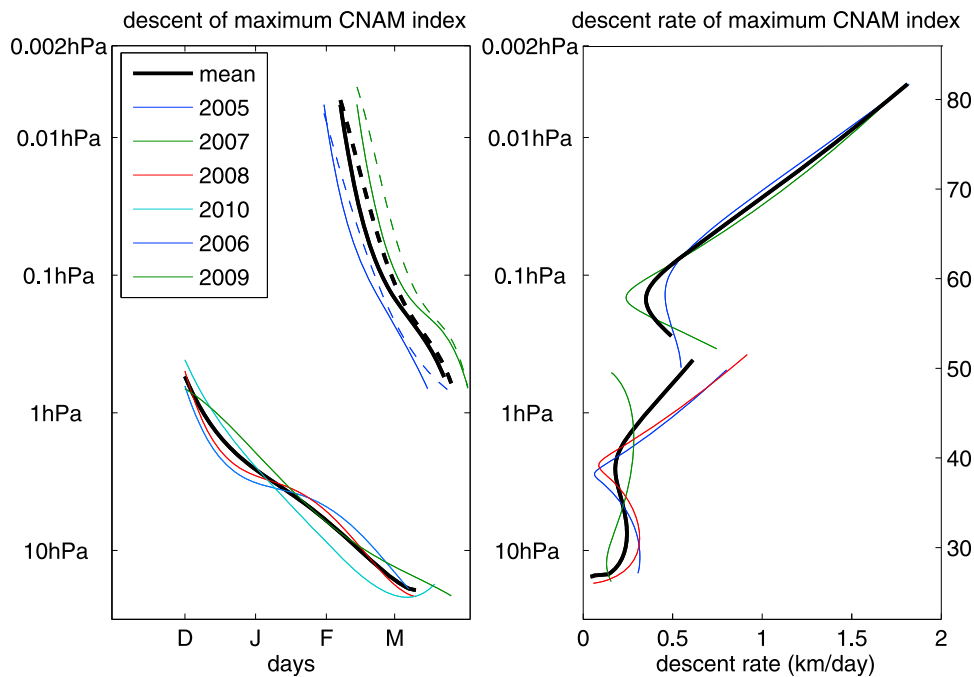


**Figure 7.** (left) Descent of the maximum CNAM index,  $P(t)$  in NH winter during 2005–2010 and (right) estimated mean descent rate of the index,  $dZ/dt$ , in km/d. Numbers on the right axis indicate geometric height in km. Values from individual winter in color and the mean in black are indicated (2005 in blue, 2006 in dark blue, 2007 in dark green, 2008 in red, 2009 in green, and 2010 in light green). Values from  $\text{H}_2\text{O}$  index maximum are also plotted with dashed lines for 2006 and 2009 winters.

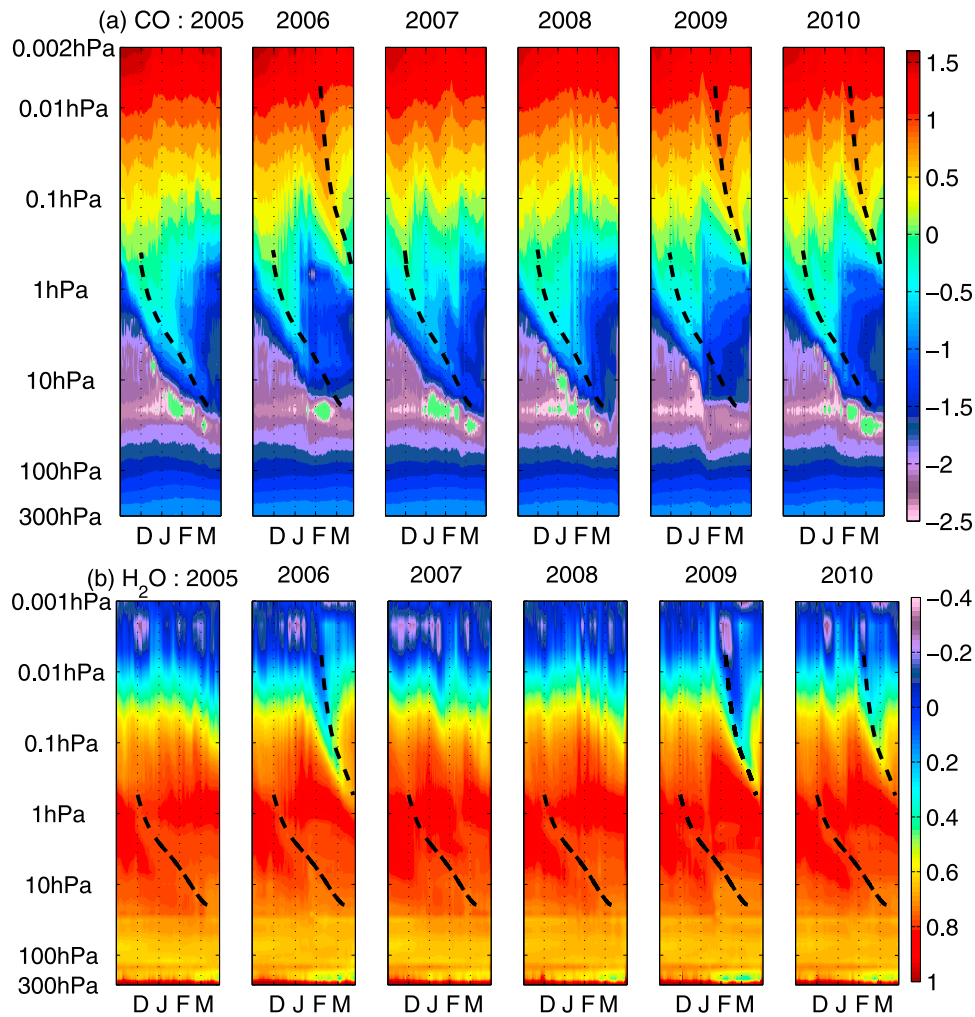


**Figure 8.** MLS high-latitude ( $60^{\circ}\text{N}$ – $82^{\circ}\text{N}$ ) zonal mean  $\text{H}_2\text{O}$  and  $\text{CO}$  volume mixing ratios in log of ppmv for 2005–2010 boreal winters. Volume mixing ratios are scaled with log to show the detailed descent to the stratosphere. Mean stratospheric descent and mean mesospheric descent of  $\text{CO}$  index,  $Z(\text{day})$ , as a regression of  $\text{CO}$  index maximum in NH winter are indicated by black lines.

0.1 hPa (60 km). The  $\text{CO}$  abundance shows maxima during the winter in the high-latitude region [Filipiak *et al.*, 2005; Jin *et al.*, 2009], which is a manifestation of the summer-to-winter meridional circulation at these altitudes and the descending air motion near the winter pole [Andrews *et al.*, 1987].

[48] In all of the strong SSW winters (2006, 2009 and 2010), the USLM  $\text{CO}$  is reduced during a short period in January, as a result of mixing into the extravortex regions and the pause in the signature of confined descent in the lower mesosphere. High  $\text{CO}$  concentrations in the upper mesosphere are seen to start descending as the mesospheric vortex reforms in late February 2006, 2009, and 2010, consistent with the CNAM development in Figure 5b. This signature of descent in January 2009 appears about one week later than in 2006. The time-height evolution of the averaged CNAM index,  $P(t)$ , captures well the mesospheric and stratospheric  $\text{CO}$  mixing ratio descent seen in Figure 8a, demonstrating that descent of the index is a good measure of the descent of  $\text{CO}$  maximum abundance. This suggests that,

in these cases, the material descent is, in fact, a dominant factor in the evolution of the CNAM index.

[49] Figure 8b shows the time-height variation of MLS  $\text{H}_2\text{O}$  averaged over a high-latitude bin ( $60^{\circ}\text{N}$ – $82^{\circ}\text{N}$ ). The time-height development of  $\text{H}_2\text{O}$  also indicates strong descent of dry air from the upper mesosphere to the upper stratosphere during both SSW winters as shown by Orsolini *et al.* [2010] with the Odin Sub-millimeter Radiometer instrument. Compared to 2006 SSW, during which humid recovery is seen in early March in the USLM, the descent after the 2009 SSW into the upper stratosphere is even more profound and prolonged, continuing until the late March. Evolution of the CNAM index,  $P(t)$ , is superposed on the averaged high-latitude  $\text{H}_2\text{O}$  contours and it represents well the mesospheric descent above 1 hPa after the SSWs in February 2006, 2009, and 2010.

[50] In the mesosphere  $\text{H}_2\text{O}$  decreases from about 6 ppmv at 0.1 hPa ( $\sim 60$  km) to about 0.5 ppmv at 0.002 hPa ( $\sim 90$  km) where it is destroyed by photolysis at Lyman  $\alpha$  wavelengths. In the stratosphere,  $\text{H}_2\text{O}$  mixing ratio increases up

to 7 ppmv due to the formation from oxidation of methane and reaches a maximum near the stratopause and lower mesosphere. The  $\text{H}_2\text{O}$  VMR decreases from the upper troposphere ( $\sim 0.35\%$  near 316 hPa) to the lower stratosphere (a few ppmv).  $\text{H}_2\text{O}$  is a good tracer for diagnosing transport in the middle atmosphere. However, it is not as good a tracer as CO for diagnosing vertical motions throughout the middle atmosphere due to the relative complexity of photochemical sources and sinks in the stratosphere. As seen in the  $\text{H}_2\text{O}$  VMR in Figure 8b,  $\text{H}_2\text{O}$  becomes less correlated with the dynamic transport below the midstratosphere compared to CO (Figure 8a).

## 4.2. Southern Hemisphere

### 4.2.1. The Southern Annular Mode

[51] Compared to the NAM, the SAM has been studied less, partly because of lack of reliable observations of GPH. In this study we apply the same algorithms as used for the NH to compute the first EOF modes for MLS GPH,  $\text{H}_2\text{O}$ , and CO, and the descent rates from the trace gases, in the SH.

[52] The first EOF mode of GPH in the SH, or SAM, is characterized by nearly zonally symmetric north-south vacillations from the midlatitude westerly jet [Kidson 1988; Karoly, 1990; Limpasuvan and Hartmann, 1999; Thompson and Wallace, 2000; Thompson *et al.*, 2005]. The SAM has a strong vertical coupling between the mesosphere and the stratosphere, as shown by the SAM index in the GPH field in Figure 9a. The high-index polarity of the SAM, defined in the same manner as for the NAM, is the period when GPH over the SH pole is anomalously low (Figure 4b). The low index polarity of the SAM is defined by anomalies in the opposite sense (Figure 4a).

[53] Figure 9a shows as much wintertime variability of the SAM index in the middle atmosphere as of the NAM during a given winter. However, in contrast to the NAM, the SAM reveals less interannual variability, showing persistence of the mode evolution throughout the whole middle atmosphere. The positive SAM phase, corresponding to a strong polar vortex and low temperatures, begins in the mesosphere (above 1 hPa) and continues for five months from May to September, progressing gradually downward into the upper stratosphere during the austral winter. The positive phase in the stratosphere (below 10 hPa) continues from July to September.

[54] A rapid change of the SAM patterns toward the negative phase occurs in late September throughout the entire mesosphere and stratosphere. The progression of the mesosphere-to-stratosphere SAM captures the relatively slow evolution of the middle and lower stratospheric vortex over  $\sim 2$  months, which coincides with the vortex breakdown by October in lower mesosphere and by late October and November in the upper stratosphere [e.g., Manney *et al.*, 2005, and references therein].

[55] The slightly negative SAM indices in 2007 winter indicates a SSW in the SH. The MLS observation shows  $\sim 20$  K increase of polar temperature ( $60^\circ\text{S}$ – $82^\circ\text{S}$ ) during mid-September 2007. The recent study of Eguchi and Kadera [2010] reports the Southern Hemisphere SSW in 2007, suggesting that the influence of the 2007 SSW extends to the tropical tropopause layer (TTL) similar to that in 2002 [Eguchi and Kadera, 2007].

### 4.2.2. Descent and Transport of Trace Gases

[56] The lack of strong SSWs in the SH in the period covered by MLS makes the CSAM index development quite different from that in the NH, leading to an uninterrupted descent in the winter polar middle atmosphere from the upper mesosphere to the middle stratosphere (Figure 10). The descent rate of the maximum CO index in the SH (CSAM index) appears to be similar for the 5 years (Figure 9b). The vortex descent starts slightly earlier in 2007 than that in 2008 and 2009. Above  $\sim 5$  hPa, the  $\text{H}_2\text{O}$  index (HSAM) shows the downward progression generally consistent with the curve inferred from the CSAM index (Figure 9c). Below 1 hPa, the negative HSAM index shows stratospheric descent slower than that in the mesosphere.

[57] There exist interannual variations in the SAM index amplitude as well in its descent rate. Above  $\sim 60$  km, as shown in Figure 10, 2006, 2007 and 2008 have a slightly larger descent rate than 2005 and 2009; whereas at  $\sim 45$  km the 2005–2006 and 2009 rates are slightly larger than 2007 and 2008. As in the NH, the descent rate of the index increases nearly linearly with altitude from 0.2 km/d at  $\sim 40$  km to 1 km/d (30 km/month) at  $\sim 80$  km. It is nearly constant in the middle and lower stratosphere below 40 km at 0.16–0.2 km/d (4.7–6 km/month). As was the case in the NH, the descent rate of the CSAM index is usually similar to the descent rate of CO mixing ratio contours averaged over the polar region (Figure 11), suggesting that descent of air in the vortex is a primary factor in controlling the CSAM evolution; however, in the fall and early winter, the downward slope of the CSAM contours is steeper than that of individual CO contours in the polar average in Figure 11, suggesting that the strengthening of the vortex at progressively lower levels is also contributing to the descent of the maximum anomaly.

[58] Early work of Fisher *et al.* [1993] explored general parcel motion of the Antarctic winter air in the stratosphere and mesosphere using winds from a 3-D model. They found that parcels initialized in the mesosphere (0.1 hPa) could descend as low as 100 hPa in the polar region over a period of 5 months, beginning in early winter. The modeled tracer distribution within the polar vortex is found to be dependent on the strength of dynamical drag in the middle atmosphere and the strength of the planetary wave forcing [Bacmeister *et al.*, 1995]. Their results using the UARS Halogen Occultation Experiment (HALOE) methane are consistent with ours that the weaker planetary wave forcing in the SH winter results in more coherent descent of long-lived tracers from the mesosphere than in the NH.

[59] Abrams *et al.* [1996a, 1996b], using data from the Atmospheric Trace Molecule Spectroscopy (ATMOS) instrument during the Atmospheric Laboratory for Science and Applications 2 (ATLAS 2) and ATLAS 3 missions, showed similar descent rates for long-lived tracers in both hemispheres ( $\sim 3.2$  km/month at 40 km), but the shorter time period of descent in the NH led to less net descent than the SH. Kawamoto and Shiotani [2000] estimate the vertical descent using  $\text{CH}_4$  profiles from UARS HALOE in the stratosphere, which yielded a value of 1.2–1.8 km/month at 0.6 ppmv (20 to 35 km).

[60] The descent rate of the CSAM index is larger (4.8–6 km/month below 40 km) than the material descent estimates from the previous studies (e.g.,  $\sim 3.2$  km/month

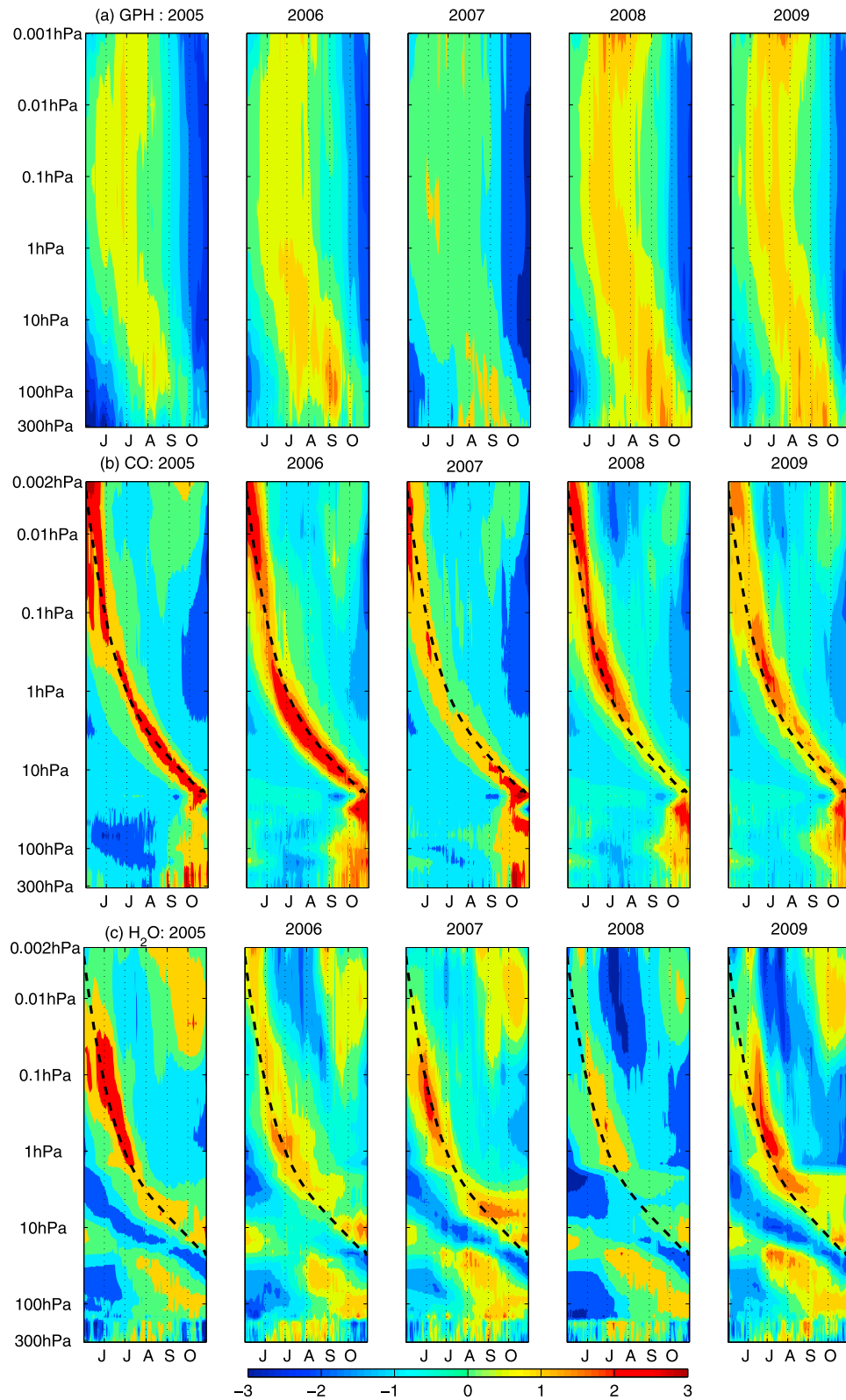


**Figure 9.** As in Figure 5 but for the SH. The 5 year mean vertical descent (black curve) is derived from the maximum CSAM index during 2005–2009 and is plotted over the HSAM index.

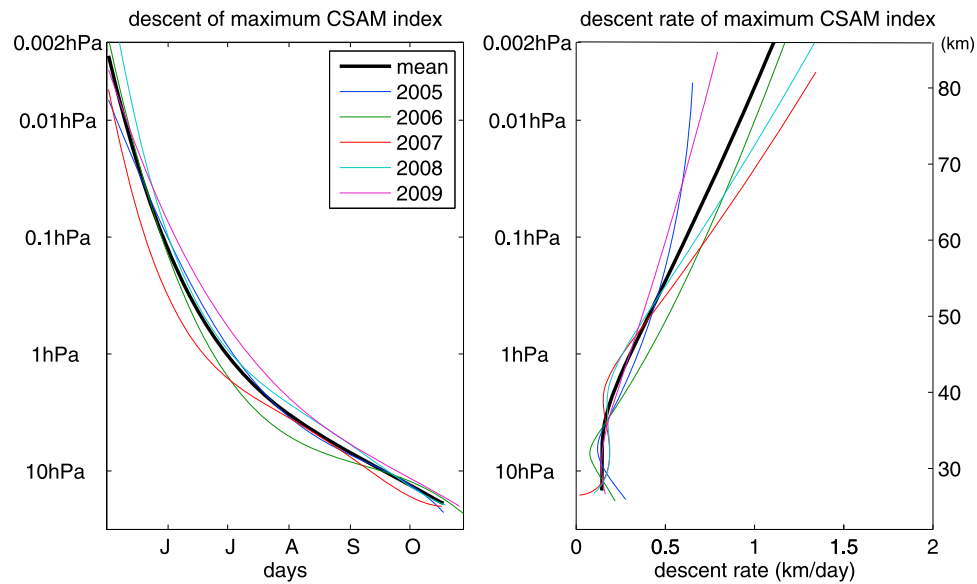


**Figure 10.** As in Figure 7 but for the SH, and values of 5 year mean descent are indicated by black lines (2005 in blue, 2006 in green, 2007 in red, 2008 in light green, and 2009 in purple).

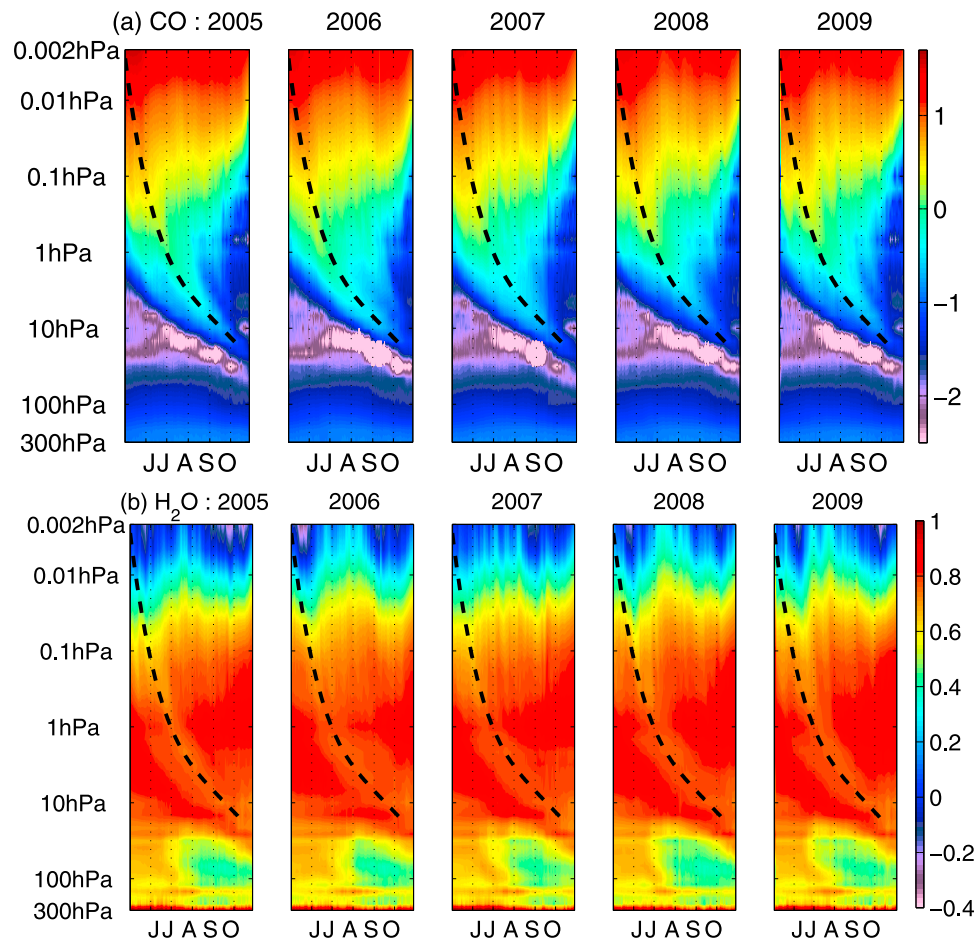


**Figure 11.** As in Figure 9 but for the SH high latitude (60°S–82°S). Values of 5 year mean descent of CO index are indicated by black lines.

from *Abrams et al.* [1996b];  $\sim 1.8$  km/month from *Kawamoto and Shiotani* [2000]). The descent rate in this study is estimated with the maximum of CO index at a certain altitude on a given day; although this does appear to usually follow the descent of maximum CO VMR averaged over high latitudes ( $60^{\circ}\text{S}$ – $82^{\circ}\text{S}$ ), a contribution from a signature of the anomaly strengthening at progressively lower levels in fall and early winter may result in the descent of the index being an overestimate of material descent. On the other hand, the earlier studies cited were severely limited by the sparseness of the data in both space and time, whereas our approach derives the descent rate of CO maximum high-latitude VMR based on the entire high-latitude CO structure during the extended winter period.

[61] The high CO VMR at high latitudes ( $60^{\circ}\text{S}$ – $82^{\circ}\text{S}$ ) is transported down to the stratosphere with a continuous downward extension of the enhancement into the lower stratosphere in each austral winter, as seen in Figure 11a. As expected from the descent of CSAM index,  $P(t)$ , monotonic descent starts near the mesopause in early winter in May and continues into the lower stratosphere until October. Evolution of CSAM index,  $P(t)$ , superposed on the averaged high-latitude CO, generally coincides closely with the mesospheric CO descent into the lower stratosphere during most of the austral winter.

[62] In Figure 11b, the zonally averaged MLS  $\text{H}_2\text{O}$  VMR over high latitude of the SH ( $60^{\circ}\text{S}$ – $82^{\circ}\text{S}$ ) shows that the mesospheric dry air is transported down to the upper stratosphere as a result of the descent inside the polar vortex.  $\text{H}_2\text{O}$  has a thick moist layer in the stratosphere between the pressure range 50 hPa to 0.1 hPa, which does not allow the transport to be observed as a vortex anomaly.

[63] Figure 8 showed that there is a gradual decrease in NH wintertime CO abundance at 0.002 hPa at a rate of  $\sim 1.8$  ppmv/yr during the boreal winter months (NDJFM) from  $\sim 30$  ppmv in 2005 to  $\sim 20$  ppmv in 2008–2010. Similarly, the mesospheric SH CO during the austral winter months (MJJASO) also decreased at a rate of  $\sim 1$  ppmv/yr from  $\sim 25$  ppmv in 2005 to  $\sim 20$  ppmv in 2009. Because mesospheric CO is transported from the lower thermosphere, where its abundance is sensitive to photolysis, this decrease is likely associated with the 11 year solar cycle. Solar cycle influences on apparent subdecadal trace gas trends are a subject of ongoing studies.

## 5. Conclusions

[64] We have analyzed the leading EOF modes of the Aura MLS GPH,  $\text{H}_2\text{O}$  and CO measurements in 2005–2010, and used the CO and  $\text{H}_2\text{O}$  annular mode indices (CNAM/CSAM, HNAM/HSAM) to characterize polar dynamics and transport in the wintertime middle atmosphere. To our knowledge, this is the first analysis of trace gases in the context of annular modes and the relationship of those features to the NAM/SAM in GPH.

[65] The first EOF of CO (CNAM and CSAM) in the middle atmosphere is an axially symmetric annular pattern which is “dome-like” shape centered on the pole, reflecting high CO VMR in high latitudes which decreases as latitude decreases. The first EOF of  $\text{H}_2\text{O}$  (HNAM and HSAM) in the mesosphere is also an annular pattern with “well-like” shape centered on the pole, reflecting a mean distribution of  $\text{H}_2\text{O}$

that is dry at high latitudes and moist at low latitudes. The positive phase of CNAM and HNAM in the mesosphere corresponds to less horizontal transport of the tracers from low to high latitudes with a well-developed polar vortex, while the negative phase corresponds to enhanced latitudinal transport and a less distinct signature of confined descent with a weaker, more permeable, polar vortex.

[66] CO acts as a good tracer of transport in the entire middle atmosphere, bringing down the high CO abundance from the lower thermosphere to the stratosphere as the vortex evolves. Descent inside the polar vortex also brings dry mesospheric air down into the upper stratosphere, but its changing gradients make its interpretation as a tracer more problematic. The evolution of NAM and SAM indices for  $\text{H}_2\text{O}$  and CO are generally consistent with each other in the mesosphere and upper stratosphere, although the reversal of the vertical gradient of  $\text{H}_2\text{O}$  due to the production from methane oxidation makes the EOF analysis complex below the stratosphere.

[67] In the NH, the vertical profiles of NAM, HNAM, and CNAM indices from MLS GPH,  $\text{H}_2\text{O}$ , and CO exhibit significant interannual variability. Our NAM analysis results show a stronger mesospheric polar vortex after significant SSWs (i.e., 2006, 2009, and 2010) than in less disturbed years. In 2006 and 2009, the strong and persistent positive HNAM and CNAM indices (or strong polar vortices) in the mesosphere are consistent with development of the positive NAM in GPH during February of 2006 and 2009. The positive NAM signals progress downward to  $\sim 1$  hPa level before the SSWs in mid-February 2006 and late February in 2009, followed by the development of a strong mesospheric NAM that progresses to the end of March of 2006 and 2009. In 2010, the positive HNAM and CNAM indices in the mesosphere are consistent with those of 2006 and 2009, but show weaker signals.

[68] The CNAM analysis reveals a significant anticorrelation ( $r = -0.9$ ) between the mesospheric and stratospheric CNAM indices from 2005 to 2010 winters. Strong mesospheric vortices (positive indices) concurrent with weak stratospheric vortices (negative indices) in late winter is thought to result from planetary-gravity wave interactions, in which planetary waves associated with SSWs prevent gravity waves from reaching the mesosphere, thus allowing the vortex to reform strongly in the upper mesosphere.

[69] An anomalously strong polar vortex leads to anomalously strong tracer gradients and thus a positive anomaly in the tracer EOF indices. Since such anomalies in vortex strength tend to propagate downward, this can contribute to the downward propagation of tracer EOF indices. Enhanced descent transports mesospheric  $\text{H}_2\text{O}$  and CO into the lower mesosphere and upper stratosphere where it remains isolated in the strong reformed polar vortex, also enhancing tracer gradients and thus strengthening the positive EOF anomalies in the tracers.

[70] In the NH, strongest CNAM index descent occurs in the mesosphere where the NAM maximum progresses downward at a rate of 1.5 km/d after the stratospheric sudden warmings (SSWs). In both mesosphere and stratosphere, the NH vortex descent is slightly faster than that in the SH with maximum difference of  $\sim 0.5$  km/d in the mesosphere and of  $\sim 0.04$  km/d in the stratosphere. The typical stratospheric index descent rate during non-SSW

winters is  $\sim 0.2$  km/d. In the SH, the strong vertical connection of the SAM suggests less interannual variability and more persistent descent from the mesosphere to stratosphere, compared to the NH.

[71] Lack of the SSW events makes the leading EOF mode development in the SH quite different from that in the NH, leading to a larger variance explained by the SAM in the mesosphere and continuous time-height evolution in the SAM index throughout the mesosphere to the upper troposphere.

[72] As in the NH, the SH CO index descent rate increases approximately linearly with altitude in the mesosphere, from  $\sim 1$  km/d at 80 km, becoming nearly constant below 40 km at about 0.16–0.2 km/d. In both hemispheres, these descent rates, estimated from the evolution of CO index, typically represent well the descent of CO from the upper mesosphere into the lower stratosphere seen in high-latitude averages, though the CSAM index descent may overestimate the material descent somewhat in fall to early winter. Further investigation is needed to determine how to more quantitatively relate descent of the CO annular mode index to material descent within the polar vortex.

[73] Knowledge of dynamics and mass transport and interannual variability in the middle atmosphere is critical to understanding variability caused by natural and anthropogenic forcings with a wide range of time scales. Disturbances in the mesosphere often influence the entire stratosphere, and can propagate further down to affect the surface via the stratosphere-troposphere coupling mechanism [Baldwin and Dunkerton, 2001]. Further investigation of interannual variability in disturbances and coupling in the middle atmosphere is thus important to understanding climate processes.

[74] Accurate amount of mesospheric CO and H<sub>2</sub>O from the MLS observation will be useful to imposing realistic upper boundary conditions in the stratospheric atmosphere models. Additional analyses of the EOF modes using model simulations (e.g., the Canadian Middle Atmosphere Model (CMAM) and the Whole-Atmosphere Community Climate Model (WACCM)), data assimilation system (DAS) analyses (e.g., CMAM DAS with online transport), and other trace gases (e.g., N<sub>2</sub>O and methane) will improve our understanding of middle atmosphere processes and coupling to the lower atmosphere, and can ultimately help improve the model physics (e.g., gravity wave parameterization) and forecast skills.

[75] **Acknowledgments.** We thank the MLS science team for their support. We also thank Varat Limpasuvan, Hanli Liu, Kunihiro Kodera, Alexander Ruzmaikin, and Joan Feynman for inspiring discussions. We would also like to acknowledge three anonymous reviewers who helped significantly improve the paper and whose comments we have adapted in the discussion. This research was supported by an appointment to the NASA Postdoctoral Program at the Jet Propulsion Laboratory, administered by Oak Ridge Associated Universities through a contract with NASA. The work at the Jet Propulsion Laboratory, California Institute of Technology, was conducted under contract with the National Aeronautics and Space Administration.

## References

- Abrams, M. C., et al. (1996a), Trace gas transport in the Arctic vortex inferred from ATMOS ATLAS-2 observations during April 1993, *Geophys. Res. Lett.*, **23**, 2345–2348, doi:10.1029/96GL00704.
- Abrams, M. C., et al. (1996b), ATMOS/ATLAS-3 Observations of trace gas transport in the Antarctic vortex in November 1994, *Geophys. Res. Lett.*, **23**, 2497–2500, doi:10.1029/96GL00705.
- Allen, D. R., et al. (1999), Observations of middle atmosphere CO from the UARS ISAMS during the early northern winter 1991/1992, *J. Atmos. Sci.*, **56**, 563–583, doi:10.1175/1520-0469(1999)056<0563:OOMACF>2.0.CO;2.
- Allen, D. R., J. L. Stanford, N. Nakamura, M. A. Lopez-Valverde, M. Lopez-Puertas, F. W. Taylor, and J. J. Remedios (2000), Antarctic polar descent and planetary wave activity observed in ISAMS CO from April to July 1992, *Geophys. Res. Lett.*, **27**, 665–668, doi:10.1029/1999GL010888.
- Andrews, D. G., J. R. Holton, and C. B. Leovy (1987), *Middle Atmospheric Dynamics*, 489 pp., Academic, San Diego, Calif.
- Bacmeister, J. T., M. R. Schoeberl, M. E. Summers, J. R. Rosenfield, and X. Zhu (1995), Descent of long-lived trace gases into the winter polar vortex, *J. Geophys. Res.*, **100**, 11,669–11,684, doi:10.1029/94JD02958.
- Baldwin, M. P., and T. J. Dunkerton (1999), Downward propagation of the Arctic oscillation from the stratosphere to the troposphere, *J. Geophys. Res.*, **104**, 30,937–30,946, doi:10.1029/1999JD900445.
- Baldwin, M. P., and T. J. Dunkerton (2001), Stratospheric harbingers of anomalous weather regimes, *Science*, **294**, 581–584, doi:10.1126/science.1063315.
- Brasseur, G. P., and S. Solomon (2005), *Aeronomy of the Middle Atmosphere*, 3rd ed., 646 pp., Springer, Dordrecht, Netherlands.
- Coy, L., S. Eckermann, and K. Hoppel (2009), Planetary wave breaking and tropospheric forcing as seen in the stratospheric sudden warming of 2006, *J. Atmos. Sci.*, **66**, 495–507, doi:10.1175/2008JAS2784.1.
- Eguchi, N., and K. Kodera (2007), Impact of the 2002 stratospheric warming in the Southern Hemisphere on the tropical cirrus clouds and convective activity, *Geophys. Res. Lett.*, **34**, L05819, doi:10.1029/2006GL028744.
- Eguchi, N., and K. Kodera (2010), Impacts of stratospheric sudden warming on tropical clouds and moisture fields in the TTL: A case study, *Sci. Online Lett. Atmos.*, **6**, 137–140, doi:10.2151/sola.2010-035.
- Eluszkiewicz, J., R. A. Plumb, and N. Nakamura (1995), Dynamics of wintertime stratospheric transport in the Geophysical Fluid Dynamics Laboratory SKYHI general circulation model, *J. Geophys. Res.*, **100**, 20,883–20,900, doi:10.1029/95JD01884.
- Filipiak, M. J., R. S. Harwood, J. H. Jiang, Q. Li, N. J. Livesey, G. L. Manney, W. G. Read, M. J. Schwartz, J. W. Waters, and D. L. Wu (2005), Carbon monoxide measured by the EOS Microwave Limb Sounder on Aura: First results, *Geophys. Res. Lett.*, **32**, L14825, doi:10.1029/2005GL022765.
- Fisher, M., A. O'Neill, and R. Sutton (1993), Rapid descent of mesospheric air in the stratospheric polar vortex, *Geophys. Res. Lett.*, **20**, 1267–1270, doi:10.1029/93GL01104.
- Flury, T., S. C. Muller, K. Hocke, and N. Kampfer (2008), Water vapor transport in the lower mesosphere of the subtropics: A trajectory analysis, *Atmos. Chem. Phys.*, **8**, 7273–7280, doi:10.5194/acp-8-7273-2008.
- Garcia, R. R., and B. A. Boville (1994), “Downward control” of the mean meridional circulation and the temperature of the polar winter stratosphere, *J. Atmos. Sci.*, **51**, 2238–2245, doi:10.1175/1520-0469(1994)051<2238:COTMMC>2.0.CO;2.
- Gerber, E. P., et al. (2010), Stratosphere-troposphere coupling and annular mode variability in chemistry-climate models, *J. Geophys. Res.*, **115**, D00M06, doi:10.1029/2009JD013770.
- Goncharenko, L. P., J. L. Chau, H.-L. Liu, and A. J. Coster (2010), Unexpected connections between the stratosphere and ionosphere, *Geophys. Res. Lett.*, **37**, L10101, doi:10.1029/2010GL043125.
- Grygalashvily, M., and G. R. Sonnemann (2006), Trends of mesospheric water vapor due to the increase of methane—A model study particularly considering high latitudes, *Adv. Space Res.*, **38**, 2394–2401, doi:10.1016/j.asr.2006.09.010.
- Harvey, V. L., C. E. Randall, and M. H. Hitchman (2009), Breakdown of potential vorticity-based equivalent latitude as a vortex-centered coordinate in the polar winter mesosphere, *J. Geophys. Res.*, **114**, D22105, doi:10.1029/2009JD012681.
- Holton, J. R., P. H. Haynes, M. E. McIntyre, A. R. Douglass, R. B. Rood, and L. Pfister (1995), Stratosphere-troposphere exchange, *Rev. Geophys.*, **33**, 403–439, doi:10.1029/95RG02097.
- Jiang, X., et al. (2008), Interannual variability and trends of extratropical ozone. Part I: Northern Hemisphere, *J. Atmos. Sci.*, **65**, 3013–3029, doi:10.1175/2008JAS2665.1.
- Jin, J. J., et al. (2009), Comparison of CMAM simulations of carbon monoxide (CO), nitrous oxide (N<sub>2</sub>O), and methane (CH<sub>4</sub>) with observations from Odin/SMR, ACE-FTS, and Aura/MLS, *Atmos. Chem. Phys.*, **9**, 3233–3252, doi:10.5194/acp-9-3233-2009.

- Karoly, D. J. (1990), The role of transient eddies in low-frequency zonal variations of the Southern Hemisphere circulation, *Tellus, Ser. A*, **42**, 41–50.
- Kawamoto, N., and M. Shiotani (2000), Interannual variability of the vertical descent rate in the Antarctic polar vortex, *J. Geophys. Res.*, **105**, 11,935–11,946, doi:10.1029/2000JD900076.
- Kidson, J. W. (1988), Interannual variations in the Southern Hemisphere circulation, *J. Clim.*, **1**, 1177–1198, doi:10.1175/1520-0442(1988)001<1177:IVTSH>2.0.CO;2.
- Lahoz, W. A., et al. (2009), Mesosphere-stratosphere transport during Southern Hemisphere autumn deduced from MIPAS observations, *Q. J. R. Meteorol. Soc.*, **135**, 681–694, doi:10.1002/qj.397.
- Lambert, A., et al. (2007), Validation of the Aura Microwave Limb Sounder middle atmosphere water vapor and nitrous oxide measurements, *J. Geophys. Res.*, **112**, D24S36, doi:10.1029/2007JD008724.
- Lee, J. N., D. L. Wu, G. L. Manney, and M. J. Schwartz (2009), Aura Microwave Limb Sounder observations of the northern annular mode: From the mesosphere to the upper troposphere, *Geophys. Res. Lett.*, **36**, L20807, doi:10.1029/2009GL040678.
- Limpasuvan, V., and D. L. Hartmann (1999), Eddies and the annular modes of climate variability, *Geophys. Res. Lett.*, **26**, 3133–3136, doi:10.1029/1999GL010478.
- Manney, G. L., R. W. Zurek, A. O'Neill, and R. Swinbank (1994), On the motion of air through the stratospheric polar vortex, *J. Atmos. Sci.*, **51**, 2973–2994, doi:10.1175/1520-0469(1994)051<2973:OTMOAT>2.0.CO;2.
- Manney, G. L., R. W. Zurek, W. A. Lahoz, R. S. Harwood, J. B. Kumer, J. Mergenthaler, A. E. Roche, A. O'Neill, R. Swinbank, and J. W. Waters (1995), Lagrangian transport calculations using UARS data. Part I: Passive tracers, *J. Atmos. Sci.*, **52**, 3049–3068, doi:10.1175/1520-0469(1995)052<3049:LTCUDP>2.0.CO;2.
- Manney, G. L., M. L. Santee, N. J. Livesey, L. Froidevaux, W. G. Read, H. C. Pumphrey, J. W. Waters, and S. Pawson (2005), EOS Microwave Limb Sounder observations of the Antarctic polar vortex breakup in 2004, *Geophys. Res. Lett.*, **32**, L12811, doi:10.1029/2005GL022823.
- Manney, G. L., et al. (2008a), The evolution of the stratopause during the 2006 major warming: Satellite data and assimilated meteorological analyses, *J. Geophys. Res.*, **113**, D11115, doi:10.1029/2007JD009097.
- Manney, G. L., et al. (2008b), The high Arctic in extreme winters: Vortex, temperature, and MLS and ACE-FTS trace gas evolution, *Atmos. Chem. Phys.*, **8**, 505–522, doi:10.5194/acp-8-505-2008.
- Manney, G. L., M. J. Schwartz, K. Krüger, M. L. Santee, S. Pawson, J. N. Lee, W. H. Daffer, R. A. Fuller, and N. J. Livesey (2009a), Aura Microwave Limb Sounder observations of dynamics and transport during the record-breaking 2009 stratospheric major warming, *Geophys. Res. Lett.*, **36**, L12815, doi:10.1029/2009GL038586.
- Manney, G. L., et al. (2009b), Satellite observations and modelling of transport in the upper troposphere through the lower mesosphere during the 2006 major stratospheric sudden warming, *Atmos. Chem. Phys.*, **9**, 4775–4795, doi:10.5194/acp-9-4775-2009.
- Minschwaner, K., et al. (2010), The photochemistry of carbon monoxide in the stratosphere and mesosphere evaluated from observations by the Microwave Limb Sounder on the Aura satellite, *J. Geophys. Res.*, **115**, D13303, doi:10.1029/2009JD012654.
- North, G. R., T. L. Bell, R. F. Cahalan, and F. J. Moeng (1982), Sampling errors in the estimation of empirical orthogonal functions, *Mon. Weather Rev.*, **110**, 699–706, doi:10.1175/1520-0493(1982)110<0699:SEITEO>2.0.CO;2.
- Offermann, D., O. Gusev, M. Donner, J. M. Forbes, M. Hagan, M. G. Mlynczak, J. Oberheide, P. Preusse, H. Schmidt, and J. M. Russell III (2009), Relative intensities of middle atmosphere waves, *J. Geophys. Res.*, **114**, D06110, doi:10.1029/2008JD010662.
- Orsolini, Y. J., J. Urban, D. P. Murtagh, S. Lossow, and V. Limpasuvan (2010), Descent from the polar mesosphere and anomalously high stratopause observed in 8 years of water vapor and temperature satellite observations by the Odin Sub-Millimeter Radiometer, *J. Geophys. Res.*, **115**, D12305, doi:10.1029/2009JD013501.
- Pancheva, D., et al. (2008), Planetary waves in coupling the stratosphere and mesosphere during the major stratospheric warming in 2003/2004, *J. Geophys. Res.*, **113**, D12105, doi:10.1029/2007JD009011.
- Pumphrey, H. C., et al. (2007), Validation of middle-atmosphere carbon monoxide retrievals from the Microwave Limb Sounder on Aura, *J. Geophys. Res.*, **112**, D24S38, doi:10.1029/2007JD008723.
- Randel, W. J., J. C. Gille, A. E. Roche, J. B. Kumer, J. L. Mergenthaler, J. W. Waters, E. F. Fishbein, and W. A. Lahoz (1993), Stratospheric transport from tropics to middle latitudes by planetary wave mixing, *Nature*, **365**, 533–535, doi:10.1038/365533a0.
- Randel, W. J., F. Wu, H. Vomel, G. E. Nedoluha, and P. Forster (2006), Decreases in stratospheric water vapor after 2001: Links to changes in the tropical tropopause and the Brewer-Dobson Circulation, *J. Geophys. Res.*, **111**, D12312, doi:10.1029/2005JD006744.
- Remsberg, E. (2010), Observed seasonal to decadal scale responses in mesospheric water vapor, *J. Geophys. Res.*, **115**, D06306, doi:10.1029/2009JD012904.
- Rosenfield, J. E., P. A. Newman, and M. R. Schoeberl (1994), Computations of diabatic descent in the stratospheric polar vortex, *J. Geophys. Res.*, **99**, 16,677–16,689, doi:10.1029/94JD01156.
- Russell, J. M., III, A. F. Tuck, L. F. Gordely, J. H. Park, S. R. Drayson, J. E. Harries, R. J. Cicerone, and P. J. Crutzen (1993), HALOE Antarctic observations in the spring of 1991, *Geophys. Res. Lett.*, **20**, 719–722, doi:10.1029/93GL00497.
- Ruzmaikin, A., and J. Feynman (2002), Solar influence on a major mode of atmospheric variability, *J. Geophys. Res.*, **107**(D14), 4209, doi:10.1029/2001JD001239.
- Salby, M., F. Sassi, P. Callaghan, D. Wu, P. Keckhut, and A. Hauchecorne (2002), Mesospheric inversions and their relationship to planetary wave structure, *J. Geophys. Res.*, **107**(D4), 4041, doi:10.1029/2001JD000756.
- Schoeberl, M. R., L. Lait, P. Newman, and J. Rosenfield (1992), The structure of the polar vortex, *J. Geophys. Res.*, **97**, 7859–7882, doi:10.1029/91JD02168.
- Schwartz, M. J., et al. (2008), Validation of the Aura Microwave Limb Sounder temperature and geopotential height measurements, *J. Geophys. Res.*, **113**, D15S11, doi:10.1029/2007JD008783.
- Siskind, D. E., S. D. Eckermann, L. Coy, and J. P. McCormack (2007), On recent interannual variability of the Arctic winter mesosphere: Implications for tracer descent, *Geophys. Res. Lett.*, **34**, L09806, doi:10.1029/2007GL029293.
- Siskind, D. E., S. D. Eckermann, J. P. McCormack, L. Coy, K. W. Hoppel, and N. L. Baker (2010), Case studies of the mesospheric response to recent minor, major and extended stratospheric warmings, *J. Geophys. Res.*, **115**, D00N03, doi:10.1029/2010JD014114.
- Solomon, S., et al. (1985), Photochemistry and transport of carbon monoxide in the middle atmosphere, *J. Atmos. Sci.*, **42**, 1072–1083, doi:10.1175/1520-0469(1985)042<1072:PATOCM>2.0.CO;2.
- Thompson, D. W. J., and J. M. Wallace (1998), The Arctic Oscillation signature in the wintertime geopotential height and temperature fields, *Geophys. Res. Lett.*, **25**, 1297–1300, doi:10.1029/98GL00950.
- Thompson, D. W. J., and J. M. Wallace (2000), Annular modes in the extratropical circulation. Part I: Month-to-month variability, *J. Clim.*, **13**, 1000–1016, doi:10.1175/1520-0442(2000)013<1000:AMITEC>2.0.CO;2.
- Thompson, D. W. J., M. P. Baldwin, and S. Solomon (2005), Stratosphere-troposphere coupling in the Southern Hemisphere, *J. Atmos. Sci.*, **62**(3), 708–715, doi:10.1175/JAS-3321.1.
- Tuck, A. F., J. M. Russell III, and J. E. Harries (1993), Stratospheric dryness: Antiphased desiccation over Micronesia and Antarctica, *Geophys. Res. Lett.*, **20**, 1227–1230, doi:10.1029/93GL00824.
- Wu, D. (2000), Mesospheric temperature inversion layers: Recent observations from UARS ISAMS and MLS, *Recent Res. Dev. Geophys.*, **3**, 37–44.

A. Lambert, J. N. Lee, N. J. Livesey, G. L. Manney, W. G. Read, M. J. Schwartz, and D. L. Wu, Jet Propulsion Laboratory, California Institute of Technology, 4800 Oak Grove Dr., Pasadena, CA 91109, USA. (jae.nyung.lee@jpl.nasa.gov)

K. R. Minschwaner, Department of Physics, New Mexico Institute of Mining and Technology, Socorro, NM 87801, USA.

H. C. Pumphrey, Institute of Atmospheric and Environmental Sciences, School of GeoSciences, University of Edinburgh, West Mains Road, Edinburgh EH9 3JN, UK.